Original Article

Enhanced anticancer activity of novel pyrimidine nucleoside analog in pancreatic cancer

Raviteja Bulusu^{1*}, Joy Okoro^{1*}, Esther Frimpong¹, Sunil Krishnan², Saunjoo Yoon³, Bo Han⁴, Xue Zhu¹, Edward Agyare¹

¹College of Pharmacy and Pharmaceutical Sciences, Institute of Public Health, Florida A&M University, Tallahassee, Florida, USA; ²Department of Neurosurgery, McGovern Medical School at The University of Texas Health Science Center at Houston, Houston, Texas, USA; ³Department of Biobehavioral Nursing Science, College of Nursing, University of Florida, Gainesville, Florida, USA; ⁴Department of Surgery, Keck School of Medicine, University of Southern California, Los Angeles, California, USA. *Equal contributors.

Received June 17, 2025; Accepted July 21, 2025; Epub August 25, 2025; Published August 30, 2025

Abstract: This study explores the synthesis, characterization, and therapeutic efficacy of AGY,, AGY,, AGY,, AGY,, AGY,, and AGY_E, which are novel 5-FU analogs designed to improve metabolic stability, prolong half-life, and anti-tumor activity against pancreatic cancer. The 5-FU molecule was chemically modified to bypass dihydropyrimidine dehydrogenase (DPD)-mediated inactivation, enhancing drug retention and increasing lipophilicity for improved cellular uptake. The analog cytotoxic activity was evaluated in 2D monolayer cultures and 3D pancreatic cancer spheroids and organoid models derived from MiaPaCa-2 and PANC-1 cells to simulate a more complex tumor environment. In the 2D model, AGY₁, AGY₂, AGY₃, AGY₄, and AGY₅ displayed significantly higher cytotoxicity than 5-FU, with AGY₂ achieving up to six-fold higher potency in MiaPaCa-2 cells. In 3D spheroid models, both AGY, and AGY, showed dose-dependent reductions in spheroid size, with AGY, causing the most pronounced shrinkage, suggesting effective disruption of the tumor architecture. In pancreatic organoids, AGY_2 demonstrated substantial decreases in cell viability and structural proliferation, inhibiting cell migration and organoid budding that exceeded the effects of 5-FU. Furthermore, cell cycle analysis revealed that AGY_2 induces significant cell cycle arrest at the $\mathsf{GO/G1}$ phase in MiaPaCa-2 cells and the S phase in PANC-1 cells. Apoptosis assays showed a higher percentage of apoptotic cells following AGY, treatment compared to 5-FU, which was supported by Western blot analysis, indicating increased expression of pro-apoptotic proteins p53 and Bax and decreased levels of survival proteins epidermal growth factor receptor (EGFR), human epidermal growth factor receptor 2 (HER-2), and Poly (ADP-ribose) polymerase (PARP). Put together, our findings showed that AGY, analog was the most effective anti-anticancer analog with significantly improved metabolic stability.

Keywords: Pancreatic cancer, 5-Fluorouracil, analogs, 2D and 3D cell models, apoptosis, Western blot

Introduction

Globally, pancreatic cancer is one of the most formidable and deadly types of soft tissue tumors, typically affecting individuals between the ages of 50 and 60 in the United States [1]. Projections for 2025 indicate that over 67,000 individuals will be diagnosed with pancreatic cancer in the United States, with an estimated 52,000 succumbing to the disease [2]. Pancreatic cancer, specifically pancreatic ductal adenocarcinoma, is an uncommon but highly aggressive malignancy with a poor prognosis, as reflected by its 5-year relative survival rate of less than 10% [3]. This stark contrast to the

improved survival rates of other common cancers, such as breast, colorectal, and prostate cancer, highlights the urgent need for advancements in effective therapeutic interventions for pancreatic cancer. The data indicates a 6.3% increase in new pancreatic cancer diagnoses and a 3.7% rise in associated mortality rates compared to 2022 figures [4]. Pancreatic cancer continues to be the fourth leading cause of cancer-related deaths in the U.S., with both its incidence and mortality rates exhibiting an upward trend since the year 2000.

By 2030, it is anticipated that pancreatic cancer will rank as the second primary contributor

80% of 5-FU follows the path of metabolism

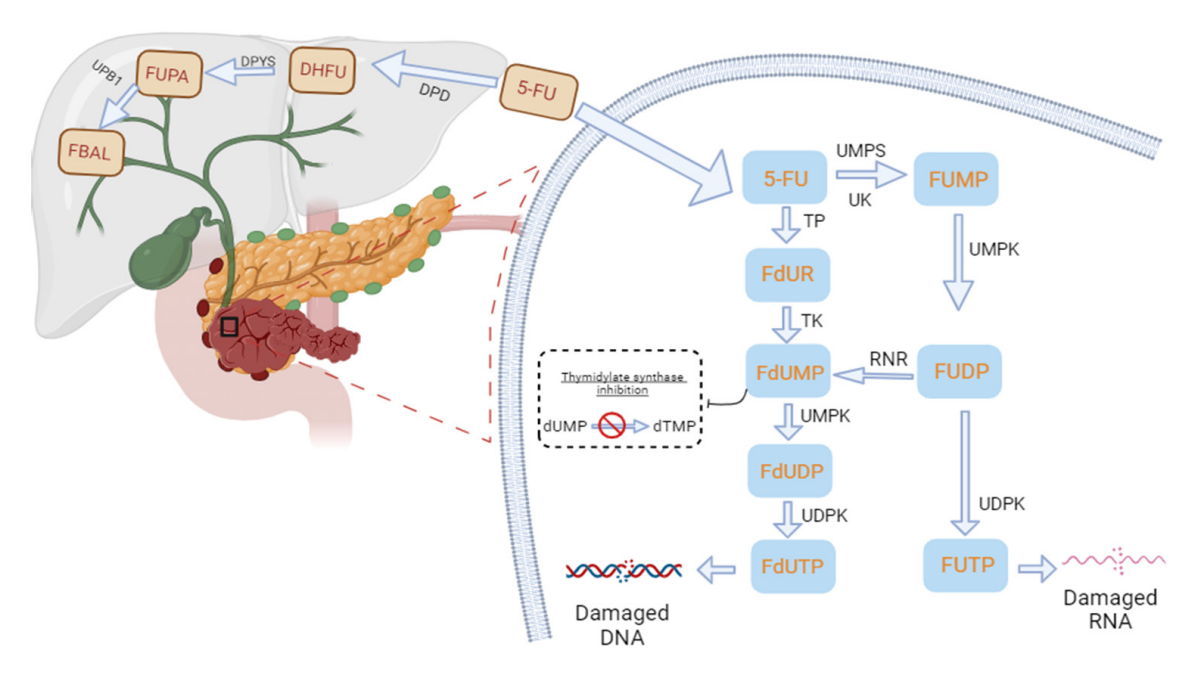


Figure 1. Mechanism of action of 5-FU. The fate of 5-FU in the system includes activation and inhibition of the synthesis of DNA or RNA, and destabilization/metabolism of 5-FU by liver enzyme (DPD).

to cancer-related fatalities in the United States, following lung cancer [5]. Pancreatic cancer originates in the tissues of the pancreas, an organ situated deep within the abdominal cavity behind the stomach [6]. The pancreas plays a critical role in the digestive system and is responsible for producing enzymes that aid in breaking down food and hormones that help regulate blood sugar levels. Pancreatic cancer is known for its aggressive nature and is often challenging to detect in its early stages, contributing to its poor prognosis. As a result, it is frequently diagnosed at an advanced stage when treatment options may be limited [7].

5-Fluorouracil (5-FU), belonging to the class of antimetabolite drugs, is a potent chemotherapeutic medication used to treat various types of cancer [8]. 5-FU, first discovered in the 1950s, has since become a cornerstone of cancer therapy and is listed on the World Health Organization's List of Essential Medicines, underscoring its significance in healthcare [9]. 5-FU is widely used to treat various cancers, including breast, colon, rectum, stomach, pancreas, and skin [10].

Once administered, 5-FU is rapidly taken up by cells via uracil-like transport mechanisms, initi-

ating its metabolic conversion. This step is followed by its conversion into substrate fluorouridine monophosphate (FUMP) or fluorodeoxyuridine (FdUR). The enzyme orotate phosphoribosyl transferase (OPRT) facilitates the conversion to FUMP in the presence of phosphoribosyl pyrophosphate (PRPP). FUMP undergoes phosphorylation to yield fluorouridine diphosphate (FUDP), which is subsequently further phosphorylated to generate either the active metabolite FUTP or fluorodeoxyuridine diphosphate (FdUDP) through the action of ribonucleotide reductase (RNR) [11]. FUTP, as a fluorinated analog of RNA nucleotide, possesses the potential to be erroneously incorporated into the RNA of cancer cells, leading to RNA damage. Given the vital role of RNAs in protein translation, the disturbed protein expression in cells treated with 5-FU triggers the cellular autophagy and apoptosis machinery [11, 12]. Simultaneously, FdUDP undergoes additional phosphorylation to form the active metabolite FdUTP, which is then integrated into the DNA of tumor cells, causing DNA damage as an alternate mechanism Figure 1.

The conversion of the prodrug 5-FU to FdUR is facilitated by the enzyme thymidine phosphorylase (TP), followed by additional phosphoryla-

tion to generate the active metabolite fluorode-oxyuridine monophosphate (FdUMP). FdUMP combines the enzyme thymidylate synthase and 5,10-methylenetetrahydrofolate (CH₂THF) to form a stable ternary complex. This complex serves as a methyl donor and irreversibly inhibits the enzymatic activity of thymidylate synthetase inhibitors. Consequently, this inhibition disrupts the conversion of the substrate deoxyuridine monophosphate (dUMP) into deoxythymidine monophosphate (dTMP), leading to imbalances in the deoxynucleotide pool. Ultimately, this cessation of cellular de novo DNA synthesis and repair occurs [13].

In the catabolic pathway, the enzyme dihydropyrimidine dehydrogenase (DPD) plays a role in the breakdown of 5-FU by converting it into 5,6-dihydro-5-fluorouracil (DHFU), an inactive metabolite. The catabolic process progresses as DHFU is transformed into α -fluoro- β -ureidopropionic acid (FUPA) through the action of dihydropyrimidinase (DPYS). Subsequent decarboxylation and deamination processes, facilitated by β -ureidopropionase (UPB1), lead to the conversion of FUPA into α -fluoro- β -alanine (FBAL) [14, 15].

The liver, where DPD is prominently expressed, plays a pivotal role, accounting for over 80% of the typical catabolism of administered 5-FU. DPD rapidly metabolizes 5-FU into inactive compounds, reducing its concentration in the bloodstream and contributing to its short halflife. Despite its challenges, 5-FU remains a critical component in treating several types of cancer and continues to play a significant role in cancer care management worldwide [13]. However, higher doses are required during administration due to the short half-life of 5-FU, resulting in systemic toxicity [16]. This systemic toxicity contributes to adverse reactions and side effects, negatively impacting human well-being [17].

Chemical modification has been recognized as one of the strategies used to address adverse drug effects or improve the therapeutic efficacy of drugs [18-20]. Therefore, in this study, we utilized chemical modification to alter the structure of 5-FU and explored the synthesis, characterization, and in vitro anticancer efficacy of 5-FU analogs (AGY₁, AGY₂, AGY₃, AGY₄, and AGY₅) in pancreatic cancer cell lines. This chemical modification aimed to render the 5-FU analogs

undetectable by DPD and prevent their metabolism into inactive forms. As previously mentioned, 5-FU functions as a prodrug, requiring conversion into active forms to manifest its anticancer activity. Following modification, these analogs transform into a double prodrug, with the anticipation that the mechanism of action of the modified 5-FU will undergo conversion to 5-FU and then to active forms of 5-FU to perform anti-cancer activity and avoid detection by DPD and subsequent metabolism. This approach aims to enhance the therapeutic efficacy of 5-FU while minimizing its systemic toxicity, thereby improving the overall treatment outcome for patients with pancreatic cancer.

Materials and methods

5-FU was purchased from AK Scientific (Union City, CA). Pancreatic cancer cell lines, Mia-PaCa-2 (ATCC® CRL-1420™) and PANC-1 (ATCC® CRL-1469™) were sourced from the American Type Culture Collection (ATCC, Manassas, VA). Human liver microsomes were purchased from ThermoFisher Scientific. All additional solvents and reagents used in the analysis were supplied by Sigma-Aldrich (St. Louis, MO).

Chemical synthesis and characterization

Preparation of chloroformate: general procedure: To a solution of alcohol (0.1 mol) and triphosgene (11.8 g, 40 mmol, 0.4 eq) in CH₂Cl₂ (40 mL) was added dropwise a solution of pyridine (8 mL) in CH2Cl2 (10 mL) at 5°C with vigorous stirring. The reaction was monitored by HNMR. After stirring for 0.5 hour at 5-10°C, icewater (100 mL) was added slowly. The organic layer was separated and followed by concentration in vacuo to remove all CH₂Cl₂. The residue was dissolved in EtOAc (200 mL). The aqueous layer was extracted with EtOAc (200 mL). The combined EtOAc layer was washed with aqueous HCI (200 mL, 5%), water (2×100 mL), then sat. NaHCO2 (100 mL), and the organic layer was dried over Na₂SO₄, then filtered. The filtrate was concentrated in vacuo and followed by distillation under vacuum to provide the chloroformate.

1-pentyl chloroformate: 1 H NMR (CDCl $_{3}$, 300 MHz) δ 4.31 (2H, t, J = 7.2 Hz), 1.68-1.78 (2H, m), 1.30-1.39 (4H, m), 0.93 (3H, t, J = 7.2 Hz).

1-heptyl chloroformate: 1 H NMR (CDCl $_{3}$, 300 MHz) δ 4.33 (2H, t, J = 7.2 Hz), 1.69-1.77 (2H, m), 1.27-1.42 (8H, m), 0.91 (3H, t, J = 6.3 Hz).

1-octyl chloroformate: 1 H NMR (CDCl₃, 300 MHz) δ 4.33 (2H, t, J = 7.2 Hz), 1.69-1.77 (2H, m), 1.26-1.42 (10H, m), 0.90 (3H, t, J = 6.3 Hz).

4-heptyl chloroformate: 1 H NMR (CDCl $_{3}$, 300 MHz) δ 4.90-4.98 (1H, m), 1.55-1.72 (4H, m), 1.30-1.53 (4H, m), 0.93 (6H, t, J = 7.2 Hz).

5-nonyl chloroformate: 1 H NMR (CDCl $_{3}$, 300 MHz) δ 4.87-4.95 (1H, m), 1,57-1.71 (4H, m), 1.27-1.34 (8H, m), 0.91 (6H, t, J = 7.2 Hz).

Synthesis of analogs

4-amino-5-fluoro-1-(tetrahydrofuran-2-yl) pyrimidin-2(1H)-one: A mixture of 5-fluorocytosine (2.0 g, 15.50 mmol), tetrahydrofuran-2-yl acetate (4.2 g, 32.31 mmol), DBU (5.0 g, 32.89 mmol) in pyridine (20 mL) was heated with stirring at 95°C for 48 hrs in a sealed flask. After cooling to room temperature, the reaction was diluted with EtOAc (400 mL) and washed with water (300×2 mL). The aqueous was collected and concentrated in vacuo to dryness. The residue was dried under vacuum for 48 hrs and followed by crystallization (MeOH/EtOAc/Hexane) to give 4-amino-5-fluoro-1-(tetrahydrofuran-2-yl) pyrimidine-2 (1H)-one, 2.25 g, in a yield of 73%.

Melting Point (M.P.) = 211-212°C.

 1 H NMR (DMSO-d⁶, 300 MHz) δ 7.71 (1H, d, J = 7.2 Hz), 7.66 (1H, brs), 7.42 (1H, brs), 5.81-5.84 (1H, m), 4.20 (1H, dd, J = 5.7, 12.9 Hz), 3.76 (1H, dd, J = 7.2, 12.9 Hz), 2.10-2.21 (1H, m), 1.80-1.94 (3H, m).

¹³C NMR (DMSO-d⁶, 151 MHz) δ 157.9 (d, J = 13.2 Hz), 153.8, 136.5 (d, J = 240.6 Hz), 125.7 (d, J = 31.2 Hz), 87.1, 69.6, 32.5, 23.9.

General procedure for synthesis of analogs (AGY1, AGY2, AGY3 AGY4 and AGY5)

Pentyl (5-fluoro-2-oxo-1-(tetrahydrofuran-2-yl)-1,2-dihydropyrimidin-4-yl) carbamate (AGY_1): To a solution of 4-amino-5-fluoro-1-(tetrahydrofuran-2-yl) pyrimidin-2(1H)-one (1.0 g, 5.02 mmol) in pyridine (10 mL) was added with stirring a solution of 1-pentyl chloroformate (0.94 g, 6.28 mmol) in $\mathrm{CH_2Cl_2}$ (5 mL) in dropwise at 0°C in 30 min. The solution was stirred at room temperature for 12 hrs. The reaction was diluted with EtOAc (300 mL) and followed by washing with sat. $\mathrm{NaHCO_3}$ (100 mL), brine (100 mL).

The Organic layer was dried with $\mathrm{Na_2SO_4}$, filtered, and concentrated in *vacuo* to dryness. The residue was purified on silica gel on an Isolera chromatograph with a gradient eluant (Hexane/EtOAc). After crystallization from EtOAc/Hexane, the afforded pentyl (5-fluoro-2-oxo-1-(tetrahydrofuran-2-yl)-1,2-dihydropyrimidin-4-yl) carbamate, 1.13 g, was obtained in a yield 7 of 2%.

Rf (Hexane/EtOAc, 1/3): 0.35.

 1 H NMR (CDCl $_{3}$, 300 MHz) δ 12.10 (1H, brs), 7.48 (1H, brs), 5.96-5.97 (1H, m), 4.23-4.27 (1H, m), 4.18 (2H, brs), 2.44 (1H, brs), 2.06-2.10 (2H, m), 1.85-1.96 (1H, m), 1.64-1.74 (2H, m), 1.36-1.40 (4H, m), 0.91-0.93 (3H, m).

¹³C NMR (CDCl₃, 151 MHz) δ 163.66, 153.60, 146.08, 139.32 (d, J = 231.1 Hz), 124.09, 88.05, 70.44, 66.49, 32.92, 28.32, 27.90, 23.63, 22.26, 14.04.

Calcd for $C_{14}H_{20}FN_3O_4$: C 53.67, H 6.43, N 13.41; Found: C 53.68, H 6.49, N 13.33.

M.P. = 91-91.5°C.

Purity is more significant than 99.6%.

 AGY_2 : ¹H NMR (CDCl₃, 300 MHz) δ: 12.12 (1H, brs), 7.50 (1H, brs), 5.94 (1H, dd, J = 1.2, 5.7 Hz), 4.24 (1H, dt, J = 3.9, 8.1 Hz), 4.16 (2H, t, J = 7.2 Hz), 3.99 (1H, dt, J = 6.6, 9.0 Hz), 2.36-2.46 (1H, m), 2.02-2.16 (2H, m), 1.84-1.94 (1H, m), 1.64-1.74 (2H, m), 1.22-1.42 (8H, m), 0.87 (3H, t, J = 6.9 Hz).

¹³C NMR (CDCl₃, 151 MHz) δ: 163.67, 153.57, 146.09, 139.34 (d, J = 234.98 Hz), 123.99, 88.04, 70.42, 66.5, 32.92, 31.65, 28.86, 28.59, 25.74, 23.63, 22.51, 13.98.

Calcd for $C_{16}H_{24}FN_3O_4$: C 56.29, H 7.09, N 12.31; Found: C 56.19, H 7.05, N 12.21.

M.P. = 98.4-98.8°C.

Purity is more significant than 99.6%.

 AGY_3 : ¹H NMR (CDCl₃, 300 MHz) δ: 12.05 (1H, brs), 7.46 (1H, brs), 5.92 (1H, dd, J = 1.5, 6.3 Hz), 4.21 (1H, dt, J = 3.9, 8.1 Hz), 4.14 (2H, t, J = 6.6 Hz), 3.99 (1H, dt, J = 6.6, 9.0 Hz), 2.32-2.46 (1H, m), 1.98-2.35 (2H, m), 1.82-1.93 (1H, m), 1.62-1.72 (2H, m), 1.19-1.42 (10H, m), 0.85 (3H, t, J = 6.6 Hz).

¹³C NMR (CDCl₃, 151 MHz) δ: 163.70, 153.60, 146.10, 139.39 (d, J = 237.33 Hz), 124.01, 88.02, 70.43, 66.52, 32.92, 31.72, 29.17, 29.11, 28.59, 25.79, 23.64, 22.57, 14.01.

Calcd for $C_{17}H_{26}FN_3O_4$: C 57.45, H 7.37, N 11.82; Found: C 57.73, H 7.52, N 11.92.

M.P. = 105.0-105.4°C.

Purity is more significant than 99.7%.

 AGY_4 : ¹H NMR (CDCl₃, 300 MHz) δ: 12.13 (1H, brs), 7.44 (1H, brs), 5.93 (1H, dd, J = 1.8, 6.6 Hz), 4.82 (1H, brs), 4.22 (1H, dt, J = 4.5, 7.8 Hz), 4.00 (1H, dt, J = 6.9, 9.0 Hz), 2.36-2.48 (1H, m), 2.02-2.10 (2H, m), 1.84-1.96 (1H, m), 1.52-1.64 (4H, m), 1.21-1.41 (8H, m), 0.86 (6H, t, J = 7.2 Hz).

¹³C NMR (CDCl₃, 151 MHz) δ: 163.55, 153.55, 146.13, 19.44 (d, J = 240.6 Hz), 123.67 (d, J = 34.6 Hz), 87.90, 76.74, 70.41, 33.85, 32.94, 27.48, 23.66, 22.56, 13.92.

Calcd for $C_{18}H_{28}FN_3O_4$: C 58.52, H 7.64, N 11.37; Found: C 58.23, H 7.67, N 11.37.

M.P. = 94.1-94.5°C.

Purity is greater than 99.5%.

 AGY_s : ¹H NMR (CDCI₃, 300 MHz) δ: 12.14 (1H, brs), 7.45 (1H, d, J = 4.8 Hz), 5.94 (1H, dd, J = 1.8, 6.3 Hz), 4.87 (1H, brs), 4.24 (1H, dt, J = 4.2, 8.4 Hz), 4.01 (1H, dt, J = 6.6, 8.7 Hz), 2.36-2.48 (1H, m), 2.01-2.60 (2H, m), 1.84-1.96 (1H, m), 1,46-1,69 (4H, m), 1.27-1.44 (4H, m), 0.91 (6H, t, J = 7.2 Hz).

¹³C NMR (CDCl₃, 151 MHz) δ: 163.55, 153.55, 146.12, 139.45 (d, J = 235.66 Hz), 123.67 (d, J = 34.28 Hz), 87.90, 76.22, 70.42, 36.31, 32.94, 23.66, 18.57, 13.89.

Calcd for $C_{16}H_{24}FN_3O_4$: C 56.29, H 7.09, N 12.31; Found: C 56.51, H 7.07, N 12.35.

M.P. = 90.8-91.2°C.

Purity is greater than 99.5%.

In-vitro cell viability

2D cell viability: Both cell lines were cultured in Dulbecco's Modified Eagle Medium (DMEM) with high glucose and L-glutamine, supple-

mented with 10% fetal bovine serum (FBS), 1% penicillin-streptomycin (PenStrep), and 2.5% 4-(2-hydroxyethyl)-1-piperazineethanesulfonic acid (HEPES).

MiaPaCa-2 and PANC-1 cells were seeded into 96-well plates at a density of 10,000 cells per well. Each drug concentration was tested in quintuplicate, and the plates were incubated at 37°C in a 5% CO₂ atmosphere. Cells were treated with various AGY₁, AGY₂, AGY₃, AGY₄, AGY₅, and 5-FU concentrations, ranging from 3.125 to 100 µM, for 48 hours. For each drug concentration, 200 µL was applied to each well in guintuplicate, and the cells were incubated for 48 hours. After the treatment, the medium was removed, and 0.5% MTT solution was added to each well. Plates were then incubated for four hours under standard conditions. Absorbance was measured with a spectrophotometer, using excitation and emission wavelengths of 560/580 nm and 590/610 nm, respectively. Cell viability percentages for each drug concentration were calculated from the absorbance data [21].

Liver microsomal stability: A 5 µM concentration of AGY, AGY, and 5-FU were incubated with human liver microsomes (HLMs) in a phosphate buffer (pH 7.4) at 37°C. The samples were then shaken at 150 rpm for a specified duration. Key parameters for the liver microsomal stability assay were optimized, including the incubation time (0-120 minutes), human liver microsome concentration (20 mg/mL), and reaction buffer composition, which included enzymatic cofactors NADP and NADPH. Control samples were prepared with the same composition as the test samples but lacked the active compounds under study. The reaction was terminated by adding 200 µL of ice-cold methanol and centrifugation at 6,000 rpm for 10 minutes. The samples were subsequently analyzed using HPLC-UV/MS. All samples were prepared in triplicate and processed according to the manufacturer's instructions (Thermo Scientific, Waltham, MA) [22].

3D spheroid

MiaPaCa-2 and PANC-1 cell lines were seeded into Nunclon Sphera® 96-well plates (Thermo Scientific, Waltham, MA) at densities of 15,000 and 12,000 cells per well, respectively, in 100 μ L of growth medium. The cells were incubated

for 48 hours to allow the formation of 3D spheroid structures. AGY_1 , AGY_2 , and 5-FU were prepared in varying concentrations (200, 100, 50, 25, 12.5, and 6.25 μ M) in a growth medium and added to the spheroids in a 1:1 ratio, followed by incubation (maintained quintuplicate per concentration). After 72 hours of treatment, spheroid diameters were measured manually using Motic image analysis software [23].

3D organoid

MiaPaCa-2 and PANC-1 cell pellets were dissociated with trypsin, adjusting cell concentrations to 2×10⁷ cells/mL. This cell suspension was mixed with a gelatin-TGase at a 1:2 volume ratio, achieving a final cell density of 5×106 cells/mL. Aliquots of 20 µL were dispensed into the wells of a 48-well plate and incubated at 37°C for 30 minutes. Matrigel was used to solidify the collagen via cross-linking, facilitating the formation of organoids. Once the collagen lattice structures were established, 500 µL of Dulbecco's Modified Eagle Medium with 10% fetal bovine serum was added, and samples were incubated at 37°C in a 5% CO atmosphere. The organoids were cultured for 48 hours to allow development, followed by a 7-day treatment with AGY_1 , AGY_2 , and 5-FU (n = 3). Images of the organoids were captured after the treatment period using a Nikon Ti Eclipse microscope [24, 25].

Cell cycle study

MiaPaCa-2 and PANC-1 cells were seeded at a density of 1×10^6 cells per T25 cm^3 flask. The cells were then incubated with varying concentrations of AGY_1 , AGY_2 , and 5-FU (0, 0.1, 0.5 & 1 μM) for 48 hours at a temperature of 37°C and a 5% CO₂ atmosphere (n = 3). After the treatment, the cells were trypsinized, gently fixed in cold 70% ethanol, added dropwise, and then stored at 4°C for 40 minutes. Following the storage period, the cells were washed twice with phosphate-buffered saline and then treated with 50 µl of RNase to digest the RNA in the sample. Subsequently, they were stained with 200 µl of propidium iodide from a 50 µg/ml stock solution for 30 minutes at room temperature in the dark to stain DNA over RNA selectively. The cell samples were filtered through a 27 ½ gauge syringe to remove any cell aggregates. The filtered cells were then analyzed using a Becton Dickinson FACSort flow cytometer with Cell-Quest software. The DNA flow cytometric analysis enabled the determination of the proportions of cells in the G1, S, and G2/M phases of the cell cycle [26].

Cell migration study

A cell migration assay was performed to assess the impact of AGY₁, AGY₂, and 5-FU on the motility of PANC-1 and MiaPaCa-2 cells. This assay used Ibidi cell culture inserts to grow cells into two confluent monolayers separated by a "wound" area. Cells were seeded into 6-well plates at a density of 14×10³ cells on each side of the insert and incubated at 37°C for 48 hours. Once the cells reached 80% confluence, adherent monolayers were formed on each side of the insert. The inserts were then carefully removed to create a gap or "wound" between the cell layers, and the monolayers were rinsed with experimental media. Cells were subsequently treated with AGY,, AGY, and 5-FU at concentrations of 3.125, 6.25, and 12.5 µM (triplicate samples were maintained). After 48 hours, images of cells migrating into the wound area were captured using a VWR fluorescence microscope [27].

Clonogenic study

To assess in vitro cell survival post-treatment, each cell line was seeded at a density of 2.0×105 cells per T25 cm3 flask and incubated at 37°C (5% CO₂, 95% humidity) until reaching 70-75% confluency. Flasks were then treated in triplicate with varying concentrations (1.5, 3, and 6 µM) of AGY₁, AGY₂, and 5-FU. On day 7, cells were trypsinized using 0.25% trypsin-EDTA, centrifuged, and the pellets were resuspended in a culture medium. PANC-1 and MiaPaCa-2 cell lines were then plated in triplicate in 6-well plates, with 1,000 live cells per well, and incubated under the same conditions. After incubation (10 days for MiaPaCa-2 and 16 days for PANC-1), formed colonies were fixed, stained, and counted, with only colonies containing at least 50 cells in the analysis [27].

Apoptosis study

MiaPaCa-2 and PANC-1 cell lines were seeded in 3D culture using Nunclon Sphera® 96-well plates (Thermo Scientific, Waltham, MA) at densities of 15,000 and 12,000 cells per 100 µL of growth medium per well, respectively. After a

Table 1. Micro-elemental analysis of novel compounds and purity (%)

		Ele	mental /	Analysis	(%)			
Analog	Theoretical				Found		Purity (%)	
	С	Н	N	С	Н	N	•	
AGY ₁	53.67	6.43	13.41	53.68	6.49	13.33	99.6	
AGY_2	56.29	7.09	12.31	56.19	7.05	12.21	99.6	
AGY_3	57.45	7.37	11.82	57.73	7.52	11.92	99.8	
AGY_4	58.52	7.64	11.37	58.23	7.67	11.37	99.5	
AGY ₅	56.29	7.09	12.31	56.51	7.07	12.35	99.5	

48-hour incubation period, the cell spheroids in each well were treated in triplicate with varying concentrations of AGY, and 5-FU (6.25-50 µM). The viability of the 3D spheroids was evaluated 72 hours post-treatment by staining them with a fluorescent dye solution containing Acridine Orange and Ethidium Bromide (5 µg/ ml). Fluorescent and brightfield images were captured using a Nikon Ti Eclipse microscope (4X magnification), with image analysis performed using NIS Elements software version 4.30.02 (Nikon Instruments Inc., Melville, NY, USA). Ratios of the fluorescent intensities for Acridine Orange versus Ethidium Bromide were calculated for each treatment concentration [28].

Western blot

MiaPaCa-2 cells were plated in a T75 flask and cultured for 2 days. Different concentrations (IC₅₀ & 2*IC₅₀) of AGY₂ and 5-FU were treated in triplicate for 48 hours. Following treatment, cells were harvested, washed with PBS, and lysed with RIPA cell lysis buffer to extract total proteins. The BCA Protein Estimation Assay Kit (Thermo Scientific) was used to determine the protein concentration. Extracted proteins were loaded onto a gel, subjected to electrophoresis. and transferred to a PVDF membrane. The blots were then cut to appropriate sizes for hybridization and incubated overnight with the rabbit primary antibody at 4°C. The following day, the primary antibody was removed and then incubated with the corresponding HRPtagged secondary antibody for 2 h at room temperature. Immune complexes were detected using an enhanced chemiluminescence solution (Bio-Rad) and visualized with the Chemi-Doc™ XRS+ imaging system (Bio-Rad). The obtained band intensities were quantified by densitometry using Image J software (NIH, USA) [29].

Statistical analysis

The results obtained from all studies were represented in mean values ± standard error of the mean (SEM). The difference between the novel analogs and 5-FU treatment groups was analyzed using one-way or two-way ANOVA or t-test, and significance was measured using Tukey's or Dunnett's mul-

tiple comparison tests between various treatment groups where necessary. Data was analyzed using GraphPad Prism 9.0 or higher (GraphPad Software, Inc., San Diego, CA, USA). This article presented results in different forms (tables, graphs, and bar charts).

Results

Chemical characterization

The analogs were synthesized in a good yield of 92%. Proton and carbon NMR were used to characterize the analogs and confirm the carbamide bonds in AGY_1 , AGY_2 , AGY_3 , AGY_4 , and AGY_5 . The purity of the compounds was determined using micro-elemental analysis, and the percentages of carbon (C), hydrogen (H), and nitrogen (N) present were determined. As shown in **Table 1** and <u>Supplementary Figures 1</u>, 2, 3, 4, 5, the percent purity of all analogs was determined to be greater than 99.5%.

Invitro cell viability

2D cell viability: The cytotoxic potential of 5-FU analogs was assessed and compared to the standard 5-FU drug using the pancreatic cancer cell lines MiaPaCa-2 and PANC-1, as determined by the MTT assay. As shown in Table 2 and Figure 2, all 5-FU analogs demonstrated higher cytotoxic activity in MiaPaCa-2 cultures. The IC₅₀ values of AGY₁, 2.15 \pm 1.3 μ M; AGY2, $2.63 \pm 1.1 \mu M$; AGY3, $10.32 \pm 0.95 \mu M$; AGY4, $6.54 \pm 1.3 \mu M$; AGY5, $4.59 \pm 0.53 \mu M$, compared to 5-FU, 12.1 ± 1.3 µM, after a 48-hour treatment. This represented a more significant cytotoxic effect for the 5-FU analog-treated groups. A similar trend was observed in the PANC-1 treated cells, where the 5-FU analogs exhibited a higher cytotoxic effect with an IC_{EQ}

Table 2. Comparison of the significant difference of IC_{50} values in pancreatic cancer cell lines after 48 hr of treatment exposure

Analog	Structure	MiaPaCa-2 (µM)	<i>p</i> -value	PANC-1 (µM)	<i>p</i> -value
5-FU	O F NH	12.1 ± 1.3	-	18.2 ± 0.9	-
AGY ₁	O NH F	2.15 ± 1.3	0.0001 (5-FU vs AGY1)	4.1 ± 1.1	0.0001 (5-FU vs AGY1)
AGY ₂	O NH F	2.63 ± 1.1	0.0001 (5-FU vs AGY2)	4.2 ± 0.84	0.0001 (5-FU vs AGY2)
AGY ₃	o o o o o o o o o o o o o o o o o o o	10.32 ± 0.95	ns (5-FU vs AGY3)	5.8 ± 0.61	0.0001 (5-FU vs AGY3)
AGY ₄	NH F	6.54 ± 1.3	0.001 (5-FU vs AGY4)	9.2 ± 1.5	0.001 (5-FU vs AGY4)
AGY ₅	O NH F	4.59 ± 0.53	0.0001 (5-FU vs AGY5)	9.1 ± 1.1	0.001 (5-FU vs AGY5)

All values are represented as mean \pm SD (n = 5). ns indicates not significant. *P \leq 0.05, **P \leq 0.01, ***P \leq 0.0001.

value of AGY $_1$ 7.1 \pm 1.1 μ M, AGY $_2$ 4.2 \pm 0.84 μ M, AGY $_3$ 5.8 \pm 0.61 μ M, AGY $_4$ 9.2 \pm 1.5 μ M, AGY $_5$ 9.1 \pm 1.1 μ M compared to 5-FU 18.2 \pm 0.9 μ M after the 48-hour treatment.

Liver microsomal stability: An in vitro liver microsomal stability assay was conducted over three hours to assess metabolic stability, comparing 5-FU, AGY_1 , and AGY_2 analogs. The results, summarized in **Figure 3**, revealed that AGY_1 and AGY_2 displayed significantly greater metabolic stability than 5-FU. Specifically, AGY_2 demonstrated the highest metabolic stability (81.8%), followed by AGY_1 (72.1%), while 5-FU showed the lowest stability at just 46.5%. This enhanced metabolic stability of AGY_2 suggests a longer half-life, which could ultimately improve its bioavailability and bolster its anticancer efficacy.

Drug-induced 3D Spheroid degradation

The effects of 5-FU, AGY₁, and AGY₂ on the degradation of 3D PANC-1 or MiaPaCa-2 spheroid

models were determined. AGY₁ and AGY₂ demonstrated a concentration-dependent decrease in spheroid size, as shown in Figure 4, where diameters of spheroids were plotted against treatment concentrations. Figure 4B and 4D show the graphical representations of diameters of treated MiaPaCa-2 and PANC-1 spheroids against different concentrations of 5-FU, AGY, and AGY, In Figure 4A, AGY, showed a remarkable decrease in the diameter of MiaPaCa-2 spheroids compared with the diameters of 5-FU and AGY,-treated MiaPaCa-2 spheroids. However, AGY, appeared to show a more reduced spheroid diameter than 5-FU-treated MiaPaCa-2 spheroids. Figure 4C shows comparable effects of AGY, and AGY, on PANC-1 spheroidal diameters, but significantly reduced spheroidal diameters compared to 5-FU-treated PANC-1.

3D organoid

AGY₁ and AGY₂ demonstrated significantly reduced organoid viability compared to

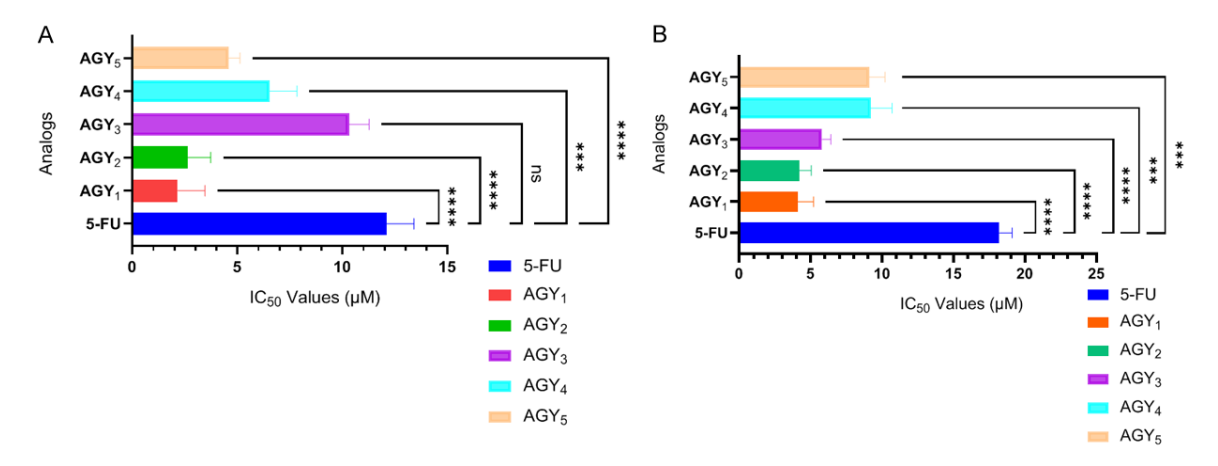


Figure 2. Graphical representation of IC_{50} values all novel compounds against (A) MiaPaCa-2 and (B) PANC-1 (2D Models).

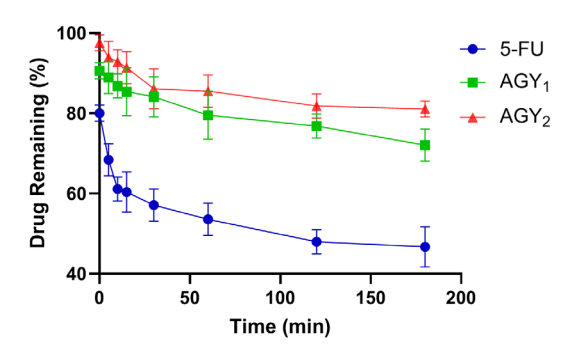


Figure 3. Metabolic stability of 5-FU, AGY₁, and AGY₂ analogs after exposure to human liver microsomal solution for 3 h. Significance was established using two-way ANOVA followed by Tukey's multiple comparison test, ***P < 0.001.

5-FU-treated organoids, with marked differences in growth patterns illustrated in Figure 5. Specifically, untreated MiaPaCa-2 and PANC-1 control organoids displayed cell migration from the central spheroid into surrounding areas, and some evidence of organoid budding and branching. 5-FU treatment, migration, and budding persisted across various concentrations with high cell confluence. In AGY1-treated organoids, the budding pattern was observed only at lower concentrations, suggesting a dose-dependent reduction in proliferative behaviour. Remarkably, AGY2-treated organoids exhibited neither migration nor budding at any concentration; instead, AGY₂ treatment caused a substantial decrease in organoid confluence. The ability of AGY₁ and AGY₂ to inhibit organoid growth more effectively than 5-FU reinforces their enhanced anti-tumor potential in 3D tumor models, suggesting they may overcome limitations associated with conventional 5-FU therapy in densely structured tumor environments.

Cell cycle study

The cell cycle profiles of MiaPaCa-2 and PANC-1 cells were analyzed to understand the stages contributing to the observed reduction in cell proliferation rates. As described in the methods section, MiaPaCa-2 and PANC-1 cells were cultured in T-25 flasks and assigned to various treatment groups. The experimental data indicate that the 5-FU analogs significantly disrupted cell cycle progression, increasing the proportion of cells arrested in different phases in both MiaPaCa-2 and PANC-1 cell lines.

In MiaPaCa-2 cells (Figure 6A and 6B), the percentage of cells in the Go/G1 phase increased with higher concentrations of the compounds. Treatment with AGY, at concentrations of 0.1 μ M, 0.5 μ M, and 1 μ M resulted in 55.1%, 66%, and 78.2% of cells being arrested in the G₂/G₃ phase, with corresponding S phase arrest resulting in 42%, 30%, and 20%, respectively. Similarly, AGY, at the same concentrations led to 52%, 58%, and 68% of cells being in the G_{\star} G, phase, with 43%, 33%, and 30% arrested in S phase, respectively. This represents a significant increase in cell cycle arrest in the G₂/G₃ phase compared to 5-FU, which had 46%, 33%, and 28% of cells in the G₂/G₄ phase, with 33%, 58%, and 60% in S phase.

In PANC-1 cells (**Figure 6C** and **6D**), AGY_1 and AGY_2 also increased the S-phase cell population arrest as the concentration increased. Specifically, at 0.1 μ M, 0.5 μ M, and 1 μ M con-

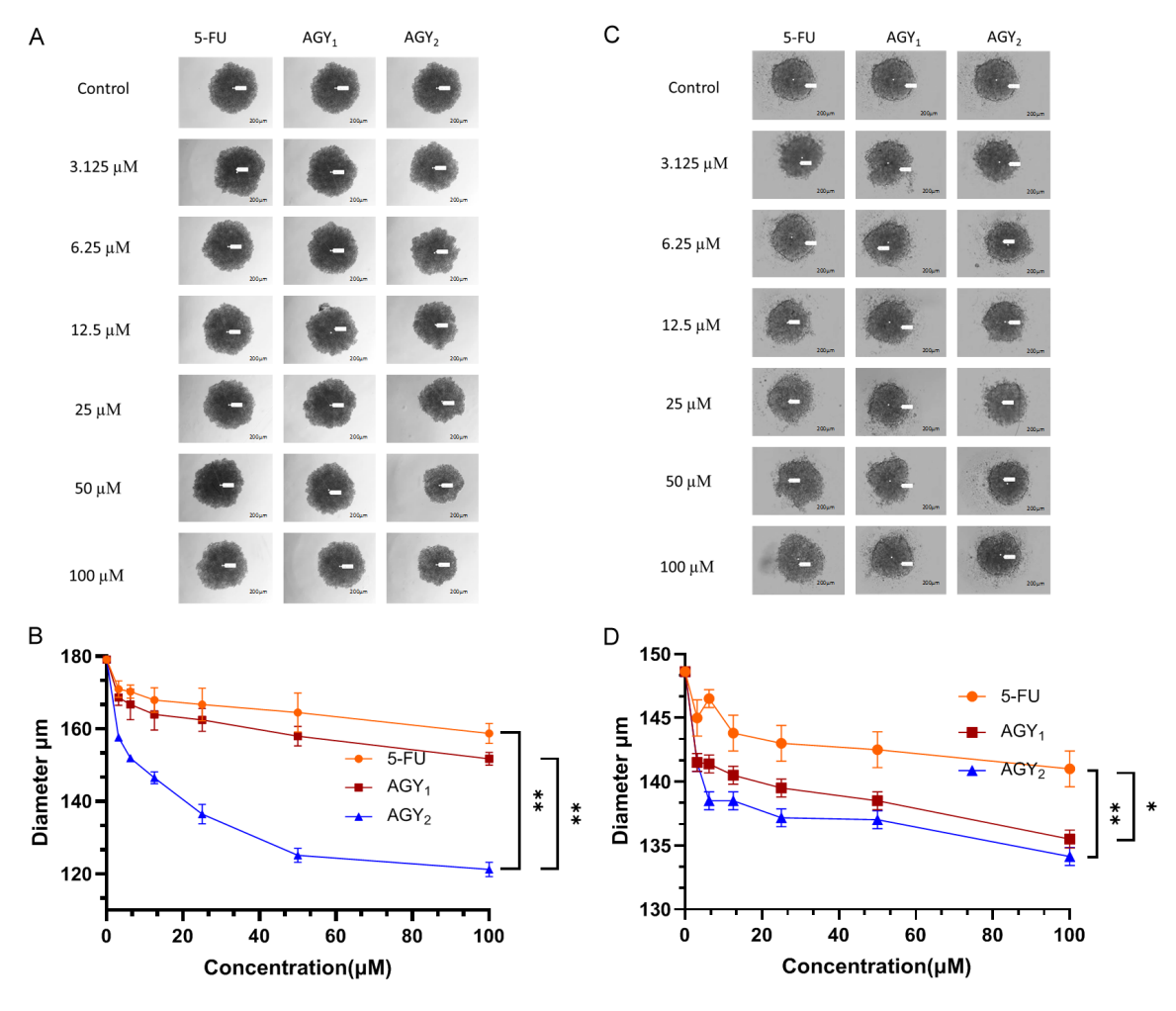


Figure 4. Images were captured for the cytotoxic effects of 5-FU, AGY $_1$, and AGY $_2$ on (A) MiaPaCa-2 and (B) PANC-1 spheroid models using an Inverted Fluorescence Microscope at 4× magnification. Graphical representations of (C) MiaPaCa-2 and (D) PANC-1 spheroidal diameters against various concentrations of 5-FU, AGY $_1$ and AGY $_2$. The level of significance difference was determined using two-way ANOVA followed by Tukey's comparison test. ** \dot{P} < 0.0035 and *P < 0.0158.

centrations of AGY_2 , 58%, 64%, and 73% of cells were arrested in the S phase, respectively. Similarly, AGY_1 resulted in 48%, 60%, and 68% of cells being arrested in the S phase, while 5-FU showed 42%, 38%, and 36% of cells in the S phase.

These findings suggest that the novel pyrimidine nucleoside analogs AGY_1 and AGY_2 exhibit enhanced anti-proliferative activity compared to 5-FU by inducing cell cycle arrest at various phases in pancreatic cancer cell lines.

Cell migration study

To evaluate the impact of the novel pyrimidine nucleoside compounds on cell migration, a

wound-healing assay was conducted using MiaPaCa-2 and PANC-1 cell lines. The cells were cultured until they reached 80% confluency, and then a wound was created in the monolayer using Ibidi inserts. Following this, the cells were treated with varying concentrations of AGY₁, AGY₂, and 5-FU.

After 24 hours of incubation, both AGY_1 and AGY_2 significantly inhibited wound closure compared to 5-FU treatment. The two analogs notably reduced the movement of cells toward the wound area, as quantified by the ImageJ software. Specifically, at concentrations of 3.125, 6.25, and 12.5 μ M, AGY_1 inhibited cell movement by 198 \pm 29, 89 \pm 13, and 74 \pm 18 cells in MiaPaCa-2 cells, and 194 \pm 16, 112 \pm 23,

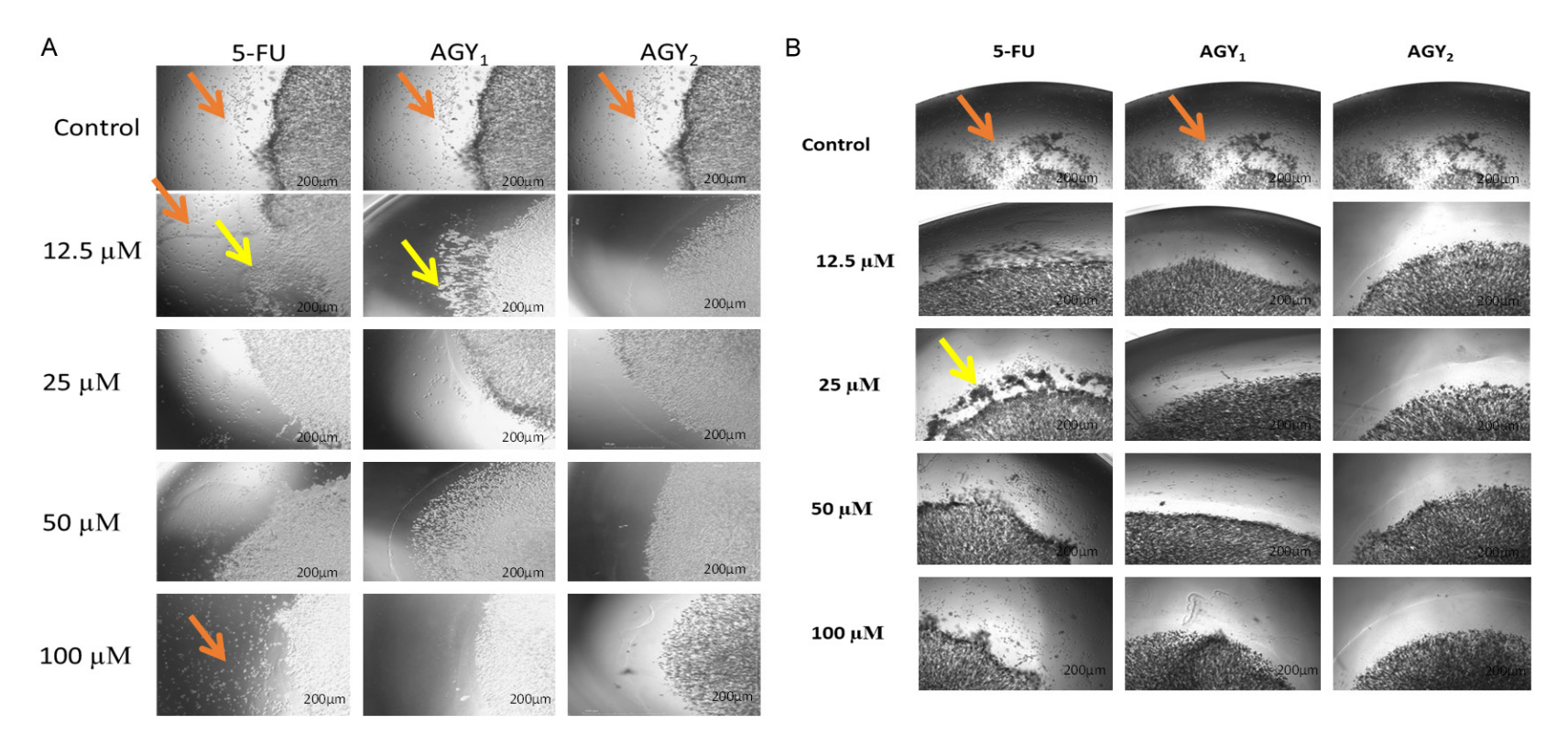
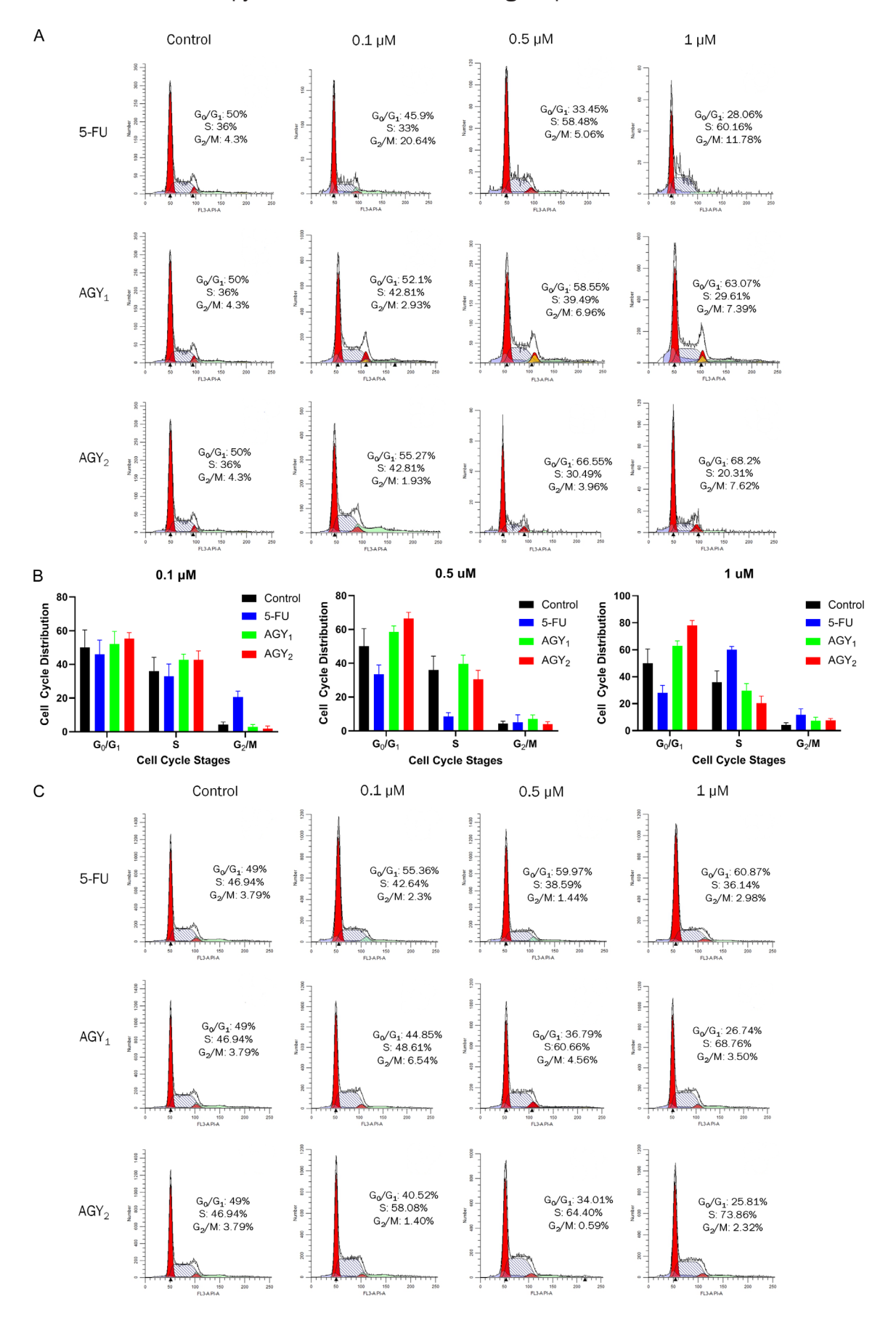
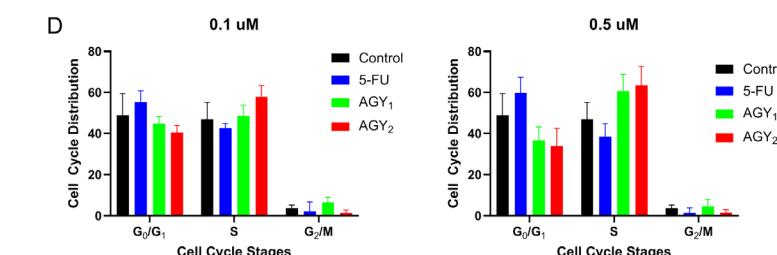


Figure 5. The cytotoxic effect of novel 5-FU analogs compared to 5-FU using organoids. (A) MiaPaCa-2 and (B) PANC-1. It demonstrates the inhibitory effect on the growth phenomena of organoids for 48 h post-treatment. All images were captured using the Nikon Ti Eclipse microscope with 4× magnification. Cell migration was represented by an orange arrow, and the yellow arrow represented organoid budding/branching.

Novel pyrimidine nucleoside analog for pancreatic cancer





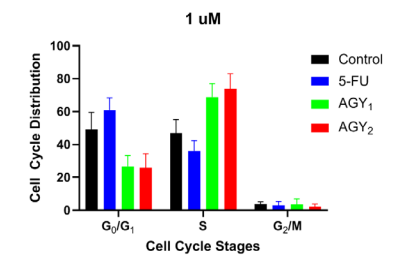


Figure 6. Analysis of cell cycle assay on pancreatic cancer cells following treatment with 5-FU analogs and 5-FU (A) MiaPaca-2 and (C) PANC-1. Graphical representations of the percentage of (B) MiaPaCa-2 and (D) PANC-1 cells arrested at different stages of the cell cycle.

and 86 ± 19 cells in PANC-1 cells, respectively (**Figure 7A-D**). Similarly, AGY2 restricted wound closure by 143 ± 11 , 65 ± 17 , and 40 ± 5 cells in MiaPaCa-2 cells and 152 ± 18 , 90 ± 20 , and 45 ± 14 cells in PANC-1 cells, respectively. In contrast, at the same concentrations, 5-FU restricted cell migration by 328 ± 42 , 209 ± 17 , and 107 ± 15 cells in MiaPaCa-2 cells and 271 ± 19 , 188 ± 15 , and 102 ± 18 cells in PANC-1 cells. The analogs showed significant concentration-dependent restriction in cell migration in both the pancreatic cancer cell lines than 5-FU.

These findings indicate that the novel pyrimidine nucleoside analogs AGY_1 and AGY_2 effectively inhibit the migration of pancreatic cancer cells in a concentration-dependent manner, highlighting their potential to mitigate metastatic spread.

Clonogenic study

A clonogenic assay was conducted to evaluate the long-term effects of the novel 5-FU analogs on the tumorigenic potential of pancreatic cancer cells. MiaPaCa-2 cells were treated with AGY₁, AGY₂, and 5-FU at various concentrations.

After 14 days of incubation, the colonies formed were stained and counted. Treatment with AGY_2 resulted in a significant decrease in the number of colonies formed compared to 5-FU. As seen in **Figure 8**, at concentrations of 1.5, 3, and 6 μ M, AGY_1 reduced colony formation by 62%, 70%, and 83%. AGY_2 reduced colony formation by 47%, 70%, and 85%, respectively, in MiaPaCa-2 cells. In contrast, 5-FU at the same concentrations only reduced colony formation by 30%, 51%, and 65%.

These results indicate that AGY₂ exhibits superior anti-proliferative and anti-tumorigenic effects compared to 5-FU in pancreatic cancer cells, highlighting its potential as a more effective therapeutic agent. The mean of triplicate values was analyzed using two-way statistical analysis, and significance was established at P < 0.0001.

Apoptosis study

Moving forward, we focused on AGY_2 due to its superior cytotoxic effect compared to AGY_1 . To further investigate the anticancer activity of the 5-FU analogs, we evaluated their capacity to induce apoptosis in pancreatic cancer cells. MiaPaCa-2 and PANC-1 cells were treated with AGY_2 and 5-FU, and apoptosis was assessed using ethidium bromide and acridine orange dyes, with acridine orange staining live cells and ethidium bromide staining dead cells. As detailed in the methods section, the intensities of the fluorescent signals were quantified using software.

As illustrated in **Figure 9**, treatment with AGY_2 resulted in a significantly higher percentage of apoptotic cells than 5-FU in both cell lines. Concurrently, the proportion of live cells decreased across all concentrations. These findings corroborate the results from the spheroid study and demonstrate that AGY_2 exhibits enhanced anticancer activity relative to the parent compound 5-FU, likely due to its improved ability to penetrate cells and tumor-like structures. The obtained values were a mean of triplicate, and using two-way ANOVA and Tukey's multiple comparison test, significance was established at P < 0.001.

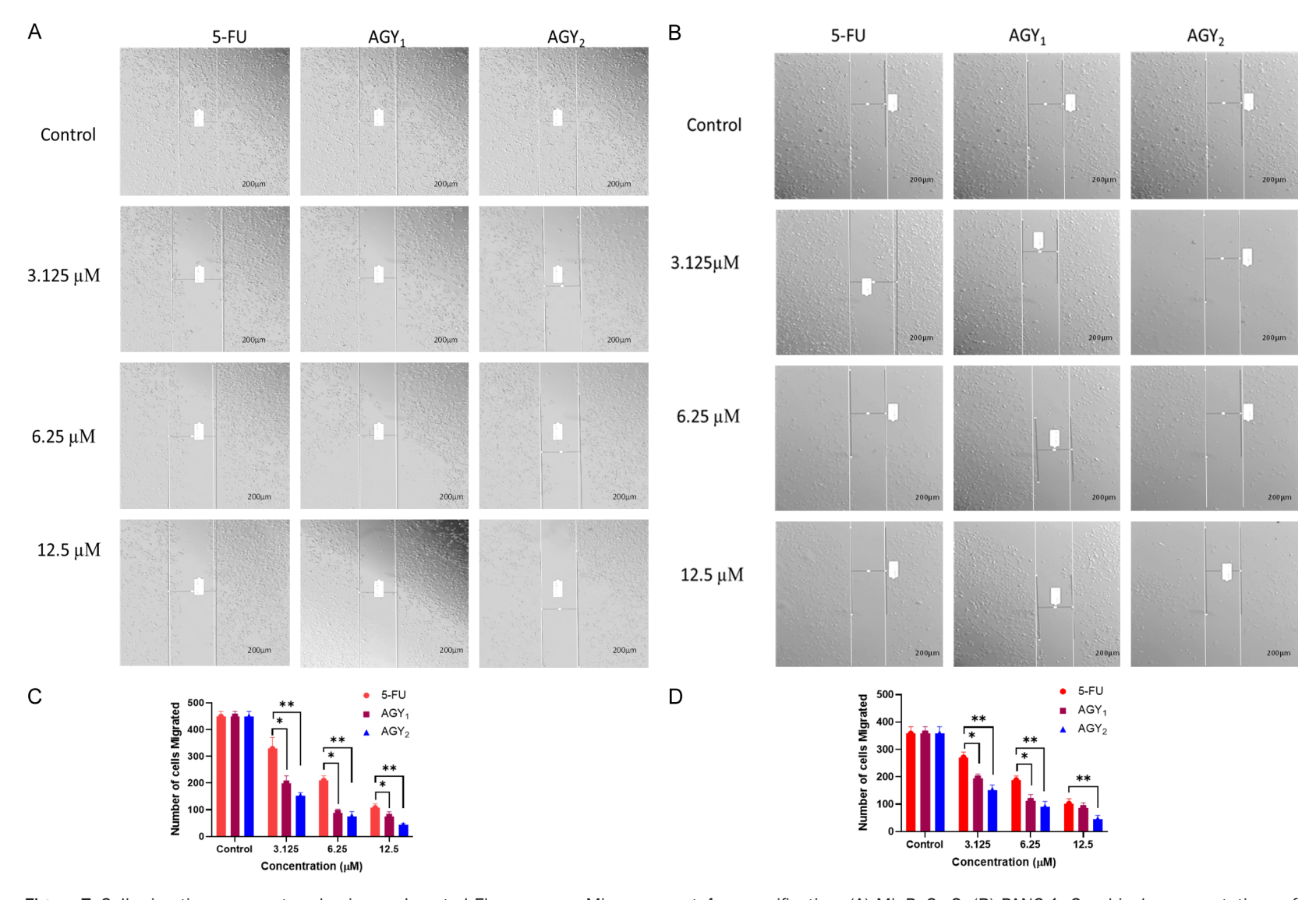
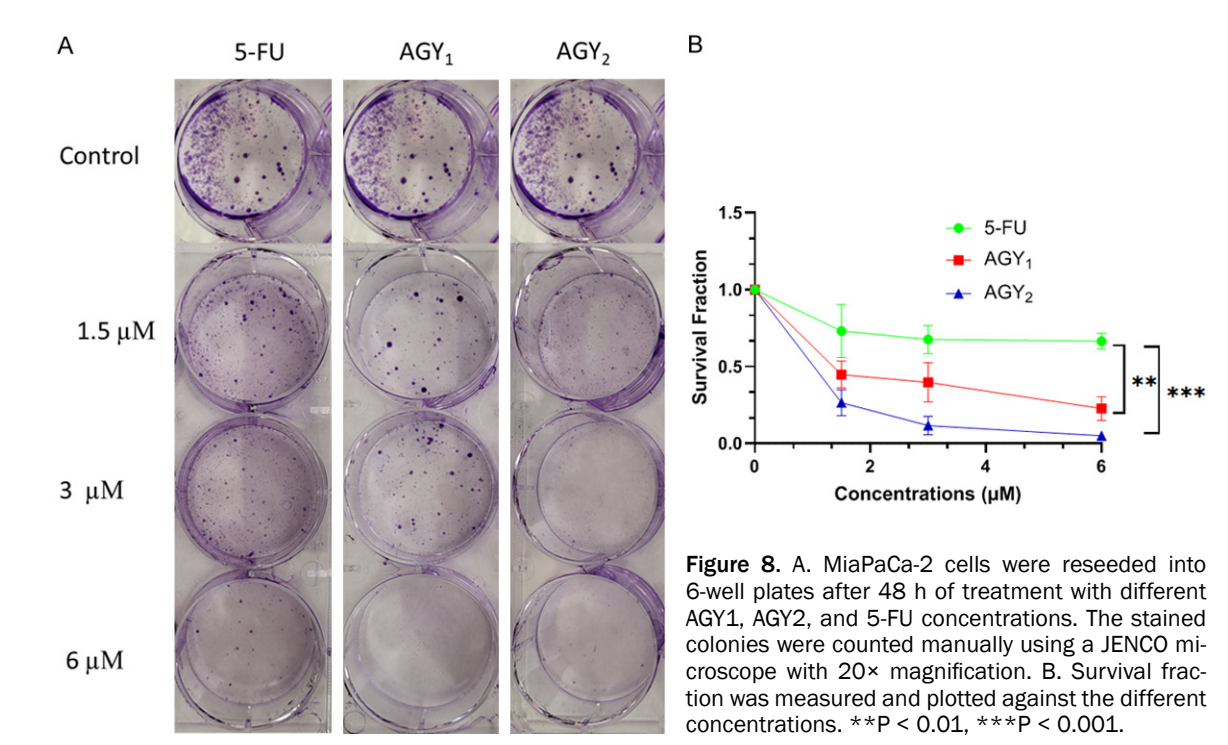


Figure 7. Cell migration was captured using an Inverted Fluorescence Microscope at $4 \times$ magnification; (A) MiaPaCa-2, (B) PANC-1. Graphical representations of migrated (C) MiaPaCa-2 and (D) PANC-1 cells towards the wound area upon treating with various concentrations of 5-FU, AGY₁, and AGY₂.



Western blot

To explore the potential molecular mechanisms underlying the enhanced anticancer activity of AGY_2 , we performed a western blot analysis to assess the expression levels of key proteins involved in cell cycle regulation and apoptosis. MiaPaCa-2 cells were treated with AGY_2 and 5-FU at different concentrations, and the expressions of proteins such as p53, VEGFR, EGFR, PARP, and BAX were examined.

As seen in Figure 10 and Supplementary Figure 6, treating MiaPaCa-2 cells with AGY, led to a significant increase in the expression of the p53 and BAX proteins as the treatment concentrations were elevated. Conversely, the levels of PARP, VEGFR, HER-2, and EGFR proteins decreased with the increasing AGY, concentrations. In comparison, 5-FU treatment caused less pronounced changes in the expression of these proteins. 5-FU treatment resulted in a relatively moderate increase in p53 and Bax expression and a pronounced decrease in PARP, VEGFR, and EGFR protein levels. These findings suggest that the improved anticancer effects of AGY, compared to 5-FU may be attributed to its ability to induce apoptosis by upregulating pro-apoptotic proteins like p53 and BAX while downregulating key growth factor receptors and survival proteins.

Discussion

FOLFIRINOX is a highly effective chemotherapeutic regimen that combines leucovorin calcium (folinic acid), 5-FU, irinotecan hydrochloride, and oxaliplatin, widely used in treating cancers such as pancreatic and colorectal cancers [30]. In pivotal randomized controlled trials, FOLFIRINOX demonstrated superior efficacy to gemcitabine in both metastatic and adjuvant settings, establishing it as a preferred option for advanced pancreatic cancer treatment [31].

Despite its effectiveness, 5-FU is rapidly metabolized upon IV administration, resulting in a short half-life (11-25 minutes) [20]. Owing to its short half-life, a higher dose is administered to achieve the therapeutic effect [32], and this dose is associated with increased cardiotoxicity risks [33], central nervous effects [17], and other adverse effects. To address this, we modified 5-FU to create analogs by masking the amine group, a key site for DPDmediated metabolism. This structural modification aims to evade rapid DPD breakdown, allowing for lower effective doses and enhancing lipophilicity, promoting passive diffusion across cell membranes for improved bioavailability and anticancer activity. Similarly, Moysan and colleagues discussed several analogs of gemcitabine to increase the stability, lipophilicity,

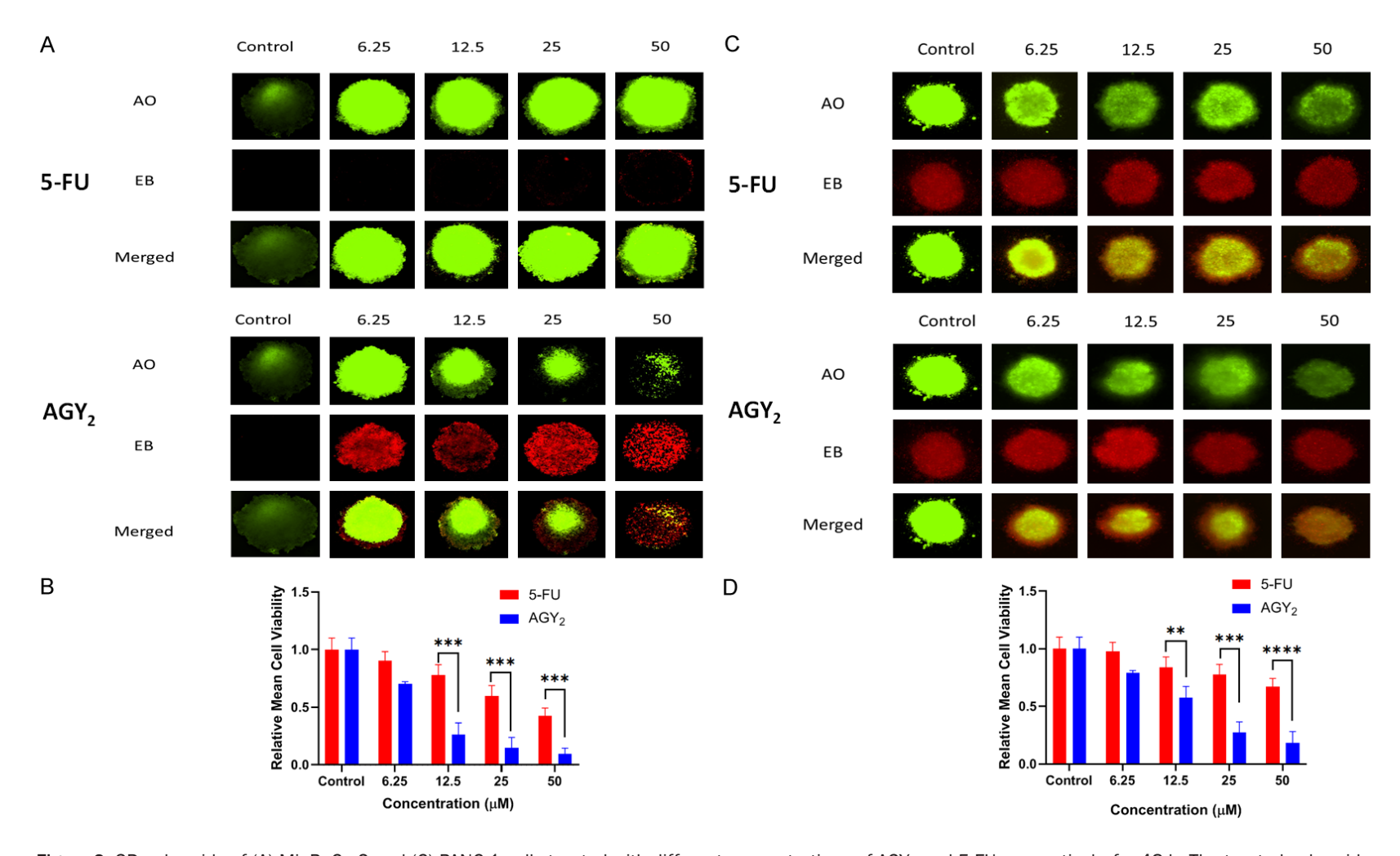


Figure 9. 3D spheroids of (A) MiaPaCa-2 and (C) PANC-1 cells treated with different concentrations of AGY $_2$ and 5-FU, respectively, for 48 h. The treated spheroids were exposed to AO and EB to stain the live and dead cells (due to apoptosis), respectively. Images were captured using a Nikon Ti Eclipse microscope (4× magnification). Graphical representation of (B) MiaPaCa-2 and (D) PANC-1 spheroids, respectively. **P < 0.001, ****P < 0.0001.

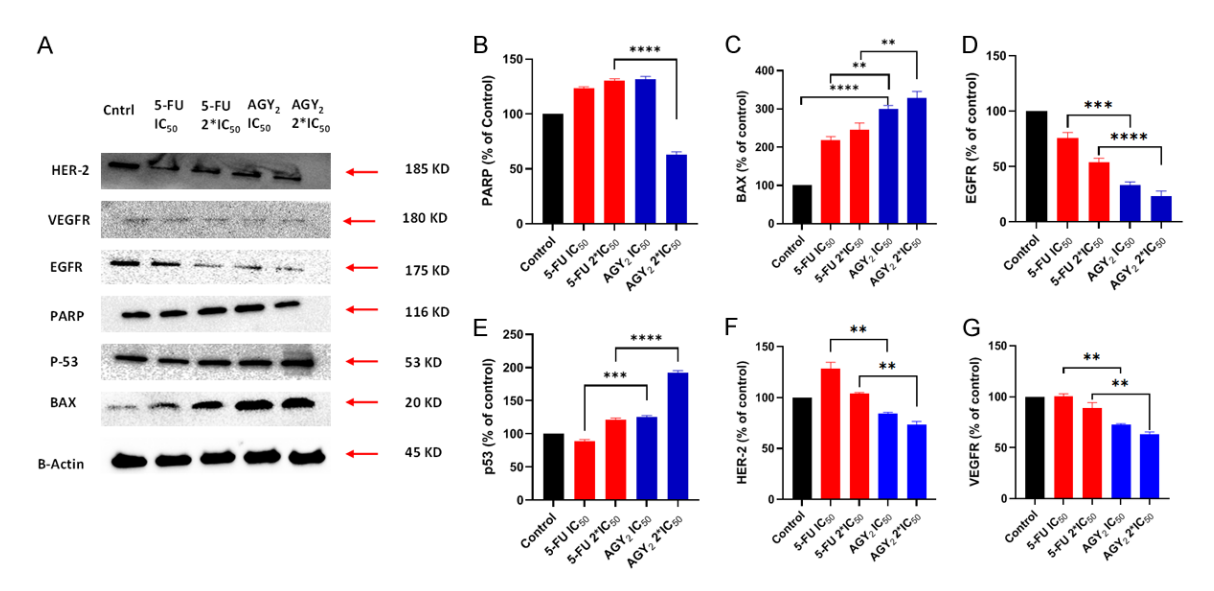


Figure 10. (A) MiaPaCa-2 cells were treated with IC $_{50}$ and double the IC $_{50}$ concentrations of AGY $_2$ and 5-FU. Total protein extract was prepared, and aliquots of 40 μg of protein extracts from different treatment groups were separated by SDS-PAGE and transferred to the PVDF membrane. Western blot analyses were performed for BAX, HER-2, VEGFR, EGFR, PARP, and p53 using specific antibodies. β-actin was used as a loading control for equal loading of proteins from figures (B-G). Quantitative densitometry was performed for each blot. **P < 0.01, ***P < 0.001, ****P < 0.0001.

and efficacy of prodrugs [34]. This approach could significantly improve the therapeutic profile of 5-FU-based treatments by minimizing toxicity while enhancing anticancer efficacy.

The newly synthesized analogs were characterized to confirm the successful conjugation of an alkyl chain at the amine position and the addition of an acetoxy tetrahydrofuran ring, which acts as a pseudo-ribose ring, as seen in **Figure 11**. This structural configuration was validated using proton and carbon Nuclear Magnetic Resonance (NMR) spectroscopy. Further, micro elemental analysis (Supplementary Figures 1, 2, 3, 4, 5) was employed to assess the compound purity by determining the percentages of C, H, and N present. This analysis demonstrated that each compound achieved a purity level exceeding 99.5%, confirming the absence of contaminants **Table 1** [35].

DPD is one of the liver microsomal enzymes that degrade 5-FU into inactive metabolites [36]. Hence, hepatic metabolic stability is a key parameter in developing 5-FU analogs because metabolic instability can prevent a drug from attaining sufficient in vivo exposure, limit the circulation time, produce short half-lives, poor oral bioavailability, and low plasma concentrations [37]. The stability of these two compounds was close to that of our previous 5-FU analog,

MFU, which has a stability of 80% [38]. This improved metabolic stability suggests that AGY₂ may have increased bioavailability and a potentially longer half-life in vivo. These findings lent credence to our hypothesis that structural modifications to 5-FU will enhance its metabolic stability, resulting in improved therapeutic efficacy and prolonged action against pancreatic cancer cells.

Following the in vitro metabolic assays, cell viability assays commenced. In 2D cell viability assays, all synthesized analogs demonstrated significantly higher cytotoxic activity than the standard drug 5-FU, as detailed in the comparative Table 1. Specifically, AGY, and AGY, exhibited nearly a six-fold increase in cytotoxic effect against MiaPaCa-2 cells, while AGY, and AGY, showed two and three-fold enhancements, respectively. A similar trend was observed in PANC-1 cells, where AGY₁ and AGY₂ were more than four times as potent as 5-FU, and AGY, and AGY, showed approximately twice the anticancer activity of 5-FU Table 2. The synthesized analogs are more cytotoxic than the existing analogs of 5-FU reported in the literature [34, 39]. Moving forward, we focused on AGY, and AGY, since they had the best cytotoxic activity after 2D cell viability assays compared to all the other analogs.

$$R = 1-C_5H_{11}, 1-C_7H_{15}, 4-C_7H_{15}, 1-C_8H_{17}, 5-C_9H_{19}$$

Reagents and conditions: i) Pyridine, DBU, 100 °C, 48 hrs; ii) Pyridine, alkyl(R) chloroformate, 0 °C - rt.

R=OH

Triphosgen, Py,
$$CH_2CI_2$$
, 0C -rt

R=OCI

R=1-C₅H₁₁, 1-C₇H₁₅, 4-C₇H₁₅, 1-C₈H₁₇, 5-C₉H₁₉

Figure 11. The synthesis of novel analogs and reaction conditions.

In 3D cell viability assays, we evaluated the antitumor potential of the analogs (AGY, and AGY₂) using complex in vitro models, such as spheroids and organoids, which better simulate the tumor microenvironment in vivo [40]. In vitro antitumor activity on spheroids is commonly represented by evaluating the ability of cells to form spheroids and analyzing their size. Spheroid size, indicative of tumor growth and treatment response, can be described in volume or diameter [41]. As shown in Figure 4, treatment with 5-FU, AGY₁, and AGY₂ significantly reduced spheroid size in both MiaPaCa-2 and PANC-1 cell lines, demonstrating an apparent concentration-dependent effect. Notably, AGY, and AGY, exhibited a more substantial inhibitory impact on spheroid growth than 5-FU at equivalent concentrations, suggesting that these analogs may have enhanced anti-tumor activity in the 3D culture model. This model, which more closely mimics the dense tumor microenvironment compared to 2D cultures, provides a valuable setting for assessing therapeutic efficacy.

More so, following the formation of MiaPaCa-2 and PANC-1 organoids, treatment with AGY₂ sig-

nificantly reduced organoid viability compared to 5-FU, with unique morphological changes and growth inhibition observed post-treatment. This reduction in organoid size and viability and the altered growth patterns suggest AGY2's enhanced ability to disrupt the structural integrity of these 3D models. AGY2's superior efficacy in reducing organoid viability compared to 5-FU highlights its potential to penetrate and act within these complex structures, possibly because of its modified structure. It may enhance cellular uptake and retention, improving its access to molecular targets within dense tumor masses.

The series of events in a cell leading to its division and duplication is called the cell cycle [42]. Dysregulation in the cell cycle can be regarded as the hallmark of cancer, or the abnormal proliferation of cells [42]. The cell cycle analysis revealed that AGY_2 and AGY_1 induced significant cell cycle arrest, particularly in the G_0/G_1 and S phases. The extent of cell cycle arrest can be modulated by adjusting the treatment concentrations and the specific cell line used [43]. In MiaPaCa-2 cells, increasing concentrations of AGY_2 led to a higher percentage of cells arrest-

ed in the G_0/G_1 phase, correlating with a decrease in the S phase population. This suggests that AGY_2 may effectively inhibit cell proliferation by preventing progression through the cell cycle, a critical aspect of cancer cell growth.

Furthermore, apoptosis is a type of genetically programmed cell death that is crucial in the development of multicellular organisms and tissues by eliminating physiologically redundant, physically damaged, and abnormal cells [44]. The induction of apoptosis was analyzed using acridine orange and ethidium bromide staining [44]. AGY₂ treatment significantly increased the percentage of apoptotic cells compared to 5-FU, indicating that AGY₂ may induce apoptosis more effectively. We postulated that this induction of apoptosis may be mediated by upregulating some pro-apoptotic proteins, such as BAX [45]. Hence, following this assay, we carried out a Western blot analysis.

Western blot analysis showed increased tumor suppressor protein p53 expression and proapoptotic protein BAX with AGY₂ treatment compared to 5-FU. The p53 protein is crucial in inhibiting phenotypic and genomic alterations associated with cancer development. Through a complex interplay involving several signaling pathways that play critical roles in essential cellular processes such as cell division, maintenance of genomic stability, apoptosis, autophagy, immune response, and regulation of tumor microenvironment, p53 can inhibit cancer development. Also, deregulated apoptosis is a hallmark of cancer as cancer cells seek to inhibit apoptosis [46]. The BAX gene encodes the BCL2L4 protein, which, upon activation, heterodimerizes with Bcl2 family proteins and alters cellular mitochondria to induce cell death [47]. Hence, increased expressions of p53 and BAX by AGY, suggest that AGY, may potentially induce higher tumor suppression and apoptosis than 5-FU.

Moreover, the expression levels of key proteins involved in cell survival and proliferation, such as EGFR, HER-2, VEGFR, and PARP (**Figure 10** and <u>Supplementary Figure 6</u>), were also examined. Overexpression of EGFR ligands results in mutations leading to increased activation of its tyrosine kinase activity, which promotes cell proliferation, differentiation, angiogenesis, and inhibition of apoptosis, thus favouring tumor growth and metastasis [48]. VEGF family

members play an essential role in developing pancreatic cancer (especially VEGF-A, VEGF-C, VEGF-D, VEGFR-1, and VEGFR-2). VEGFR-2 is the most crucial receptor in evaluating angiogenesis in pancreatic cancer, and VEGF overexpression may be considered a diagnostic marker and a poor prognostic factor of pancreatic cancer [49]. Similarly, HER2, which is a receptor tyrosine kinase, has been overexpressed in some cases of pancreatic cancer, and overexpression of HER2 is associated with poor clinical outcomes of this disease [50]. In our western blot assay, AGY, treatment decreased these proteins' levels, suggesting a mechanism where AGY, induces apoptosis and downregulates pathways that promote cell survival and proliferation. Specifically, we note that while AGY, treatment correlates with increased expression of pro-apoptotic proteins (p53, Bax) and decreased expression of growth-promoting receptors (EGFR, HER-2, VEGFR), it is not yet fully elucidated whether these effects are direct molecular actions of AGY₂ or downstream consequences of apoptosis. Future mechanistic studies, such as knockdowns or upstream pathway inhibition, could help delineate these effects [51].

Cell migration is vital for immune response, normal development, and disease processes such as cancer metastasis and inflammation [52]. The migration assay demonstrated that AGY_1 and AGY_2 significantly inhibited cell migration in the PANC-1 and MiaPaCa-2 cell lines. The ability of these analogs to restrict cell movement toward the wound area indicates their potential to prevent metastatic spread, a critical challenge in pancreatic cancer treatment. The reduced migration suggests that AGY_1 and AGY_2 may interfere with the signaling pathways that govern cell motility, thereby impairing the ability of cancer cells to invade surrounding tissues.

Additionally, the clonogenic assay, which is an in vitro cell survival assay based on the ability of a single cell to grow into a colony [53], showed that AGY_2 significantly reduced both the number and size of colonies formed by MiaPaCa-2 cells compared to 5-FU. This indicated that AGY_2 may possess superior antitumorigenic effects compared to 5-FU, as it inhibits immediate cell proliferation and impacts cancer cells' long-term survival and growth potential. The ability to inhibit colony

formation is crucial, suggesting that ${\rm AGY}_2$ could effectively prevent tumor recurrence and metastasis.

Conclusion

This study highlights the enhanced anticancer activity of AGY, compared to 5-FU in pancreatic cancer cell lines. The improved metabolic stability, superior anti-proliferative effects in 3D models, induction of apoptosis, and inhibition of cell migration collectively underscore the therapeutic potential of AGY2. These findings suggest that AGY, could serve as a promising candidate for further development as a treatment for pancreatic cancer. Future studies will focus on elucidating the molecular mechanisms underlying the action of AGY2, including its interactions with specific cellular targets, signaling pathways involved in apoptosis, and cell cycle regulation. In vivo studies, which are crucial in assessing the efficacy and safety of AGY, in more complex biological systems, will also be conducted. Such investigations will help establish the clinical relevance of AGY, as a novel therapeutic agent for pancreatic cancer, to improve treatment outcomes and patient survival rates.

Disclosure of conflict of interest

None.

Address correspondence to: Dr. Edward Agyare, Division of Pharmaceutical Sciences, 1415 South Martin Luther King Blvd, Tallahassee, Florida 32307, USA. Tel: 850-599-3581; Fax: 850-599-3934; E-mail: edward.agyare@famu.edu

References

- [1] Goggins M, Overbeek KA, Brand R, Syngal S, Del Chiaro M, Bartsch DK, Bassi C, Carrato A, Farrell J, Fishman EK, Fockens P, Gress TM, van Hooft JE, Hruban RH, Kastrinos F, Klein A, Lennon AM, Lucas A, Park W, Rustgi A, Simeone D, Stoffel E, Vasen HFA, Cahen DL, Canto MI and Bruno M; International Cancer of the Pancreas Screening (CAPS) consortium. Management of patients with increased risk for familial pancreatic cancer: updated recommendations from the International Cancer of the Pancreas Screening (CAPS) Consortium. Gut 2020; 69: 7-17.
- [2] Siegel RL, Kratzer TB, Giaquinto AN, Sung H and Jemal A. Cancer statistics, 2025. CA Cancer J Clin 2025; 75: 10-45.
- [3] Sarantis P, Koustas E, Papadimitropoulou A, Papavassiliou AG and Karamouzis MV. Pancre-

- atic ductal adenocarcinoma: treatment hurdles, tumor microenvironment and immunotherapy. World J Gastrointest Oncol 2020; 12: 173-181.
- [4] Siegel RL, Miller KD, Fuchs HE and Jemal A. Cancer statistics, 2022. CA Cancer J Clin 2022; 72: 7-33.
- [5] Rahib L, Smith BD, Aizenberg R, Rosenzweig AB, Fleshman JM and Matrisian LM. Projecting cancer incidence and deaths to 2030: the unexpected burden of thyroid, liver, and pancreas cancers in the United States. Cancer Res 2014; 74: 2913-2921.
- [6] Schwingel J, Decker M, Schneider L, Stürmer CJ and Lutz MP. Early detection of pancreatic cancer. Oncol Res Treat 2023; 46: 259-267.
- [7] Caban M and Małecka-Wojciesko E. Gaps and opportunities in the diagnosis and treatment of pancreatic cancer. Cancers (Basel) 2023; 15: 5577.
- [8] Valencia-Lazcano AA, Hassan D, Pourmadadi M, Shamsabadipour A, Behzadmehr R, Rahdar A, Medina DI and Díez-Pascual AM. 5-Fluorouracil nano-delivery systems as a cutting-edge for cancer therapy. Eur J Med Chem 2023; 246: 114995.
- [9] Zhang N, Yin Y, Xu SJ and Chen WS. 5-Fluorouracil: mechanisms of resistance and reversal strategies. Molecules 2008; 13: 1551-1569.
- [10] Vodenkova S, Buchler T, Cervena K, Veskrnova V, Vodicka P and Vymetalkova V. 5-fluorouracil and other fluoropyrimidines in colorectal cancer: past, present and future. Pharmacol Ther 2020; 206: 107447.
- [11] Azwar S, Seow HF, Abdullah M, Faisal Jabar M and Mohtarrudin N. Recent updates on mechanisms of resistance to 5-fluorouracil and reversal strategies in colon cancer treatment. Biology (Basel) 2021; 10: 854.
- [12] Yao CW, Kang KA, Piao MJ, Ryu YS, Fernando PMDJ, Oh MC, Park JE, Shilnikova K, Na SY, Jeong SU, Boo SJ and Hyun JW. Reduced autophagy in 5-fluorouracil resistant colon cancer cells. Biomol Ther (Seoul) 2017; 25: 315-320.
- [13] Ghafouri-Fard S, Abak A, Tondro Anamag F, Shoorei H, Fattahi F, Javadinia SA, Basiri A and Taheri M. 5-Fluorouracil: a narrative review on the role of regulatory mechanisms in driving resistance to this chemotherapeutic agent. Front Oncol 2021; 11: 658636.
- [14] Albadari N, Xie Y and Li W. Deciphering treatment resistance in metastatic colorectal cancer: roles of drug transports, EGFR mutations, and HGF/c-MET signaling. Front Pharmacol 2024; 14: 1340401.
- [15] Longley DB, Harkin DP and Johnston PG. 5-fluorouracil: mechanisms of action and clinical strategies. Nat Rev Cancer 2003; 3: 330-338.

- [16] Li S, Wang A, Jiang W and Guan Z. Pharmacokinetic characteristics and anticancer effects of 5-fluorouracil loaded nanoparticles. BMC Cancer 2008; 8: 103.
- [17] Han R, Yang YM, Dietrich J, Luebke A, Mayer-Pröschel M and Noble M. Systemic 5-fluorouracil treatment causes a syndrome of delayed myelin destruction in the central nervous system. J Biol 2008; 7: 12.
- [18] Araújo F, Martins C, Azevedo C and Sarmento B. Chemical modification of drug molecules as strategy to reduce interactions with mucus. Adv Drug Deliv Rev 2018; 124: 98-106.
- [19] Juillerat-Jeanneret L and Schmitt F. Chemical modification of therapeutic drugs or drug vector systems to achieve targeted therapy: looking for the grail. Med Res Rev 2007; 27: 574-590.
- [20] Frimpong E, Bulusu R, Okoro J, Inkoom A, Ndemazie N, Rogers S, Zhu X, Han B and Agyare E. Development of novel pyrimidine nucleoside analogs as potential anticancer agents: synthesis, characterization, and In-vitro evaluation against pancreatic cancer. Eur J Pharm Sci 2024; 196: 106754.
- [21] van Meerloo J, Kaspers GJ and Cloos J. Cell sensitivity assays: the MTT assay. Methods Mol Biol 2011; 731: 237-245.
- [22] Wang X, He B, Shi J, Li Q and Zhu HJ. Comparative proteomics analysis of human liver microsomes and S9 fractions. Drug Metab Dispos 2020; 48: 31-40.
- [23] Chen W, Wong C, Vosburgh E, Levine AJ, Foran DJ and Xu EY. High-throughput image analysis of tumor spheroids: a user-friendly software application to measure the size of spheroids automatically and accurately. J Vis Exp 2014; 89: e51639.
- [24] Han B. Screening miRNA for functional significance by 3D cell culture system. Methods Mol Biol 2018; 1733: 193-201.
- [25] Matthys OB, Silva AC and McDevitt TC. Engineering human organoid development ex vivochallenges and opportunities. Curr Opin Biomed Eng 2020; 13: 160-167.
- [26] Selliah N, Nash V, Eck S, Green C, Oldaker T, Stewart J, Vitaliti A and Litwin V. Flow cytometry method validation protocols. Curr Protoc 2023; 3: e868.
- [27] Inkoom A, Ndemazie NB, Smith T, Frimpong E, Bulusu R, Poku R, Zhu X, Han B, Trevino J and Agyare E. Biological evaluation of novel gemcitabine analog in patient-derived xenograft models of pancreatic cancer. BMC Cancer 2023; 23: 435.
- [28] Al-kawmani AA, Alanazi KM, Farah MA, Ali MA, Hailan WAQ and Al-Hemaid FMA. Apoptosis-inducing potential of biosynthesized silver nanoparticles in breast cancer cells. J King Saud Univ Sci 2020; 32: 2480-2488.

- [29] Kalvala AK, Nimma R, Bagde A, Surapaneni SK, Patel N, Arthur P, Sun L, Singh R, Kommineni N, Nathani A, Li Y and Singh M. The role of cannabidiol and tetrahydrocannabivarin to overcome doxorubicin resistance in MDA-MB-231 xenografts in athymic nude mice. Biochimie 2023; 208: 19-30.
- [30] Chevalier H, Vienot A, Lièvre A, Edeline J, El Hajbi F, Peugniez C, Vernerey D, Meurisse A, Hammel P, Neuzillet C, Borg C and Turpin A. FOLFIRINOX De-Escalation in advanced pancreatic cancer: a multicenter real-life study. Oncologist 2020; 25: e1701-e1710.
- [31] Conroy T, Desseigne F, Ychou M, Bouché O, Guimbaud R, Bécouarn Y, Adenis A, Raoul JL, Gourgou-Bourgade S, de la Fouchardière C, Bennouna J, Bachet JB, Khemissa-Akouz F, Péré-Vergé D, Delbaldo C, Assenat E, Chauffert B, Michel P, Montoto-Grillot C and Ducreux M; Groupe Tumeurs Digestives of Unicancer; PRODIGE Intergroup. FOLFIRINOX versus gemcitabine for metastatic pancreatic cancer. N Engl J Med 2011; 364: 1817-1825.
- [32] Gusella M, Crepaldi G, Barile C, Bononi A, Menon D, Toso S, Scapoli D, Stievano L, Ferrazzi E, Grigoletto F, Ferrari M and Padrini R. Pharmacokinetic and demographic markers of 5-fluorouracil toxicity in 181 patients on adjuvant therapy for colorectal cancer. Ann Oncol 2006; 17: 1656-1660.
- [33] Faheem B, Kania B, Ashkar H, Bondili L and Maroules M. 5-Fluorouracil-related cardiotoxicity with coronary vasospasms. J Community Hosp Intern Med Perspect 2022; 12: 71-74.
- [34] Moysan E, Bastiat G and Benoit JP. Gemcitabine versus modified gemcitabine: a review of several promising chemical modifications. Mol Pharm 2013; 10: 430-444.
- [35] Bird M, Keitel C and Meredith W. Analysis of biochars for C, H, N, O and S by elemental analyser. Biochar: A guide to analytical methods 2017; 39-50.
- [36] Fidai SS, Sharma AE, Johnson DN, Segal JP and Lastra RR. Dihydropyrimidine dehydrogenase deficiency as a cause of fatal 5-Fluorouracil toxicity. Autops Case Rep 2018; 8: e2018049.
- [37] Siramshetty VB, Shah P, Kerns E, Nguyen K, Yu KR, Kabir M, Williams J, Neyra J, Southall N, Nguyễn ĐT and Xu X. Retrospective assessment of rat liver microsomal stability at NCATS: data and QSAR models. Sci Rep 2020; 10: 20713.
- [38] Ndemazie NB, Inkoom A, Ebesoh D, Bulusu R, Frimpong E, Trevino J, Han B, Zhu X and Agyare E. Synthesis, characterization, and anticancer evaluation of 1,3-bistetrahydrofuran-2yl-5-FU as a potential agent for pancreatic cancer. BMC Cancer 2022; 22: 1345.

Novel pyrimidine nucleoside analog for pancreatic cancer

- [39] Kaya Çakir H and Eroglu O. In vitro anti-proliferative effect of capecitabine (Xeloda) combined with mocetinostat (MGCD0103) in 4T1 breast cancer cell line by immunoblotting. Iran J Basic Med Sci 2021; 24: 1515-1522.
- [40] Nayak P, Bentivoglio V, Varani M and Signore A. Three-dimensional in vitro tumor spheroid models for evaluation of anticancer therapy: recent updates. Cancers (Basel) 2023; 15: 4846.
- [41] Thakuri PS, Gupta M, Plaster M and Tavana H. Quantitative size-based analysis of tumor spheroids and responses to therapeutics. Assay Drug Dev Technol 2019; 17: 140-149.
- [42] Almalki SG. The pathophysiology of the cell cycle in cancer and treatment strategies using various cell cycle checkpoint inhibitors. Pathol Res Pract 2023; 251: 154854.
- [43] Sakaue-Sawano A, Kobayashi T, Ohtawa K and Miyawaki A. Drug-induced cell cycle modulation leading to cell-cycle arrest, nuclear missegregation, or endoreplication. BMC Cell Biol 2011: 12: 2.
- [44] Liu K, Liu PC, Liu R and Wu X. Dual AO/EB staining to detect apoptosis in osteosarcoma cells compared with flow cytometry. Med Sci Monit Basic Res 2015; 21: 15-20.
- [45] Peña-Blanco A and García-Sáez AJ. Bax, Bak and beyond mitochondrial performance in apoptosis. FEBS J 2018; 285: 416-431.
- [46] Lopez A, Reyna DE, Gitego N, Kopp F, Zhou H, Miranda-Roman MA, Nordstrøm LU, Narayanagari SR, Chi P, Vilar E, Tsirigos A and Gavathiotis E. Co-targeting of BAX and BCL-XL proteins broadly overcomes resistance to apoptosis in cancer. Nat Commun 2022; 13: 1199.

- [47] Zha H, Aimé-Sempé C, Sato T and Reed JC. Proapoptotic protein Bax heterodimerizes with Bcl-2 and homodimerizes with Bax via a novel domain (BH3) distinct from BH1 and BH2. J Biol Chem 1996: 271: 7440-7444.
- [48] Press MF and Lenz HJ. EGFR, HER2 and VEGF pathways: validated targets for cancer treatment. Drugs 2007; 67: 2045-2075.
- [49] Costache MI, Ioana M, Iordache S, Ene D, Costache CA and Săftoiu A. VEGF Expression in pancreatic cancer and other malignancies: a review of the literature. Rom J Intern Med 2015; 53: 199-208.
- [50] Shibata W, Kinoshita H, Hikiba Y, Sato T, Ishii Y, Sue S, Sugimori M, Suzuki N, Sakitani K, Ijichi H, Mori R, Endo I and Maeda S. Overexpression of HER2 in the pancreas promotes development of intraductal papillary mucinous neoplasms in mice. Sci Rep 2018; 8: 6150.
- [51] Blondy S, David V, Verdier M, Mathonnet M, Perraud A and Christou N. 5-Fluorouracil resistance mechanisms in colorectal cancer: from classical pathways to promising processes. Cancer Sci 2020; 111: 3142-3154.
- [52] Justus CR, Leffler N, Ruiz-Echevarria M and Yang LV. In vitro cell migration and invasion assays. J Vis Exp 2014; 51046.
- [53] Franken NA, Rodermond HM, Stap J, Haveman J and van Bree C. Clonogenic assay of cells in vitro. Nat Protoc 2006; 1: 2315-2319.

Sample No 6180 Atlantic E Norcross, GA www.atlanticm	AGY ₁ Blvd. Suite M 30071 icrolab.com		Dept Address City State Zin	ny/School Florida A&M Univ College of Pharmacy		
PO# / CC#			Name	Xue You Zhu Date 11/04/2020		
Element	Theory	Fo	und	Single Duplicate		
С	53.67	53.68		Elements Present: C14H20FN3O4 Analyze		
Н	6.43	6.49		for: CHN		
N	13.41	13.33		Hygroscopic Explosive M.P.		
				Include Email Address or FAX # Below xue.zhu@famu.edu		
Date Received	DEC 01	2020	Date Cor	DEC 02 2020		

Supplementary Figure 1. Micro-elemental analysis of AGY_1 showing the percent by mass of the elements carbon, hydrogen and nitrogen in the structure compared to theoretical estimates.

Sample No	AGY ₂		Compar	ny/School Florida A&M Univ College of Pharmacy		
180 Atlantic B Norcross, GA www.atlanticm	30071		Dept Address			
Professor/Supervisor:			Name .	Xue You Zhu	Date 10/15/202	
Element	Theory	Fot	ind	Single	Duplicate	
С	56.29	56.19		Present: Analyze	C16H24FN3O4	
Н	7.09	7.05		for:	CHN	
N	12.31	12.21		M.P. To be dried: Ye Temp. rt Rush Service	Vac. yes Time 24 h	
					.zhu@famu.edu	

Supplementary Figure 2. Micro-elemental analysis of AGY_2 showing the percent by mass of the elements carbon, hydrogen and nitrogen in the structure compared to theoretical estimates.

Atlantic Microlab, Inc. Sample No. Florida A&M Univ Company/School ___ 6180 Atlantic Blvd. Suite M College of Pharmacy Dept. Norcross, GA 30071 Address www.atlanticmicrolab.com City, State, Zip. Xue You Zhu Date 02/09/2022 Dr Agyare Name Professor/Supervisor: FAM01-0000207176 Phone PO# / CC#. Single Duplicate Element Theory Found C17H26FN3O4 Elements 57.73 С 57.45 Present: CHN 7.52 7.37 Н Hygroscopic Explosive 11.92 11.82 To be dried: Yes No Temp, rt Vac. yes Include Email Address or FAX # Belo

Supplementary Figure 3. Micro-elemental analysis of AGY₃ showing the percent by mass of the elements carbon, hydrogen and nitrogen in the structure compared to theoretical estimates.

Date Completed

FEB 1 0 2022

Date Received

Remarks:

Remarks:

xue.zhu@famu.edu FEB 1 4 2022

Atlantic Microlab, Inc. AGY₄ Sample No. Florida A&M Univ Company/School, 6180 Atlantic Blvd. Suite M College of Pharmacy Dept. Norcross, GA 30071 Address www.atlanticmicrolab.com City, State, Zip. Andriana Date 10/15/2021 Dr Agyare Name. Professor/Supervisor: FAM01-0000195546 PO# / CC#_ Phone Duplicate Single Element Theory C18H28FN3O4 Elements 58.23 58.52 C CHN 7.67 Н 7.64 Explosive M.P. B.P. To be dried: Yes No Temp. Vac. Yes Time 11.37 Ν 11.37 xue.zhu@famu.edu OCT 2 1 2021 OCT 2 0 2021 Date Completed

Supplementary Figure 4. Micro-elemental analysis of AGY₄ showing the percent by mass of the elements carbon, hydrogen and nitrogen in the structure compared to theoretical estimates.

Atlantic Microlab, Inc. Sample No. Florida A&M Univ Company/School_ 6180 Atlantic Blvd. Suite M College of Pharmacy Dept. Norcross, GA 30071 www.atlanticmicrolab.com Address City, State, Zip. Dr Agyare Name Date___, Professor/Supervisor: FAM01-0000207176 PO# / CC#. Phone Single __ Duplicate Element Theory Found Elements Present: C16H24FN3O4 56.51 С 56.29 Analyze for: CHN 7.07 7.09 Н Hygroscopic Explosive B.P. To be dried; Yes No Temp. Yes. Was. Wes Irrue Rush Service Rush service sonaled and insola and is on the day to surface for one the day to surface the surface. 12.35 Ν 12.31 on the day the sample is received by 11 AM. Include Email Address or FAX # Below

Supplementary Figure 5. Micro-elemental analysis of AGY_5 showing the percent by mass of the elements carbon, hydrogen and nitrogen in the structure compared to theoretical estimates.

Date Completed

FEB 1 0 2022

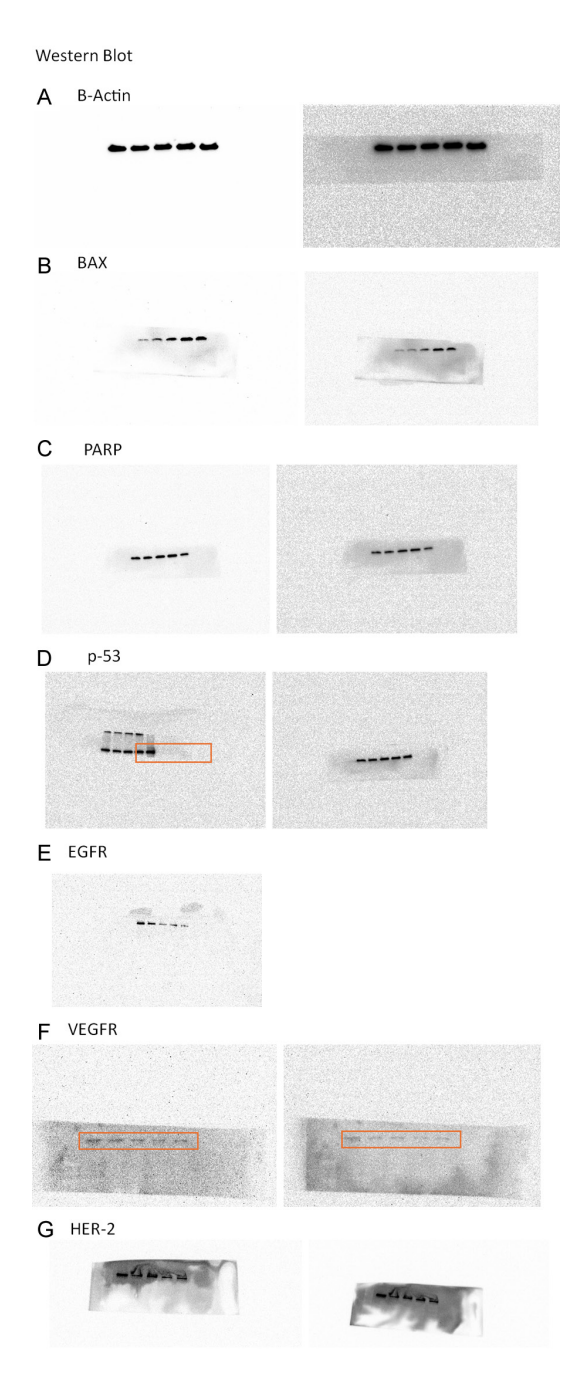
Date Received

Remarks:

xue.zhu@famu.edu

FEB 1 4 2022

Novel pyrimidine nucleoside analog for pancreatic cancer



Supplementary Figure 6. Uncropped Western blot images (A-G) used for quantitative analysis.